Universidade Estadual de Campinas
Faculdade de Engenharia Química

LETICIA FRIGERIO CREMASCO

OPERANDO CHARACTERIZATION OF LI-O_2 BATTERIES: THE EFFECT OF REDOX MEDIATORS

CARACTERIZAÇÃO *OPERANDO* DE BATERIAS LI-O_2: O EFEITO DOS MEDIADORES REDOX

CAMPINAS
2021

LETICIA FRIGERIO CREMASCO

OPERANDO CHARACTERIZATION OF Li-O_2 BATTERIES: THE EFFECT OF REDOX MEDIATORS

CARACTERIZAÇÃO *OPERANDO* DE BATERIAS Li-O_2: O EFEITO DOS MEDIADORES REDOX

Thesis presented to the Faculty of Chemical Engineering of the University of Campinas in fulfillment of the requirements for the degree of Doctor in Chemical Engineering.

Tese apresentada à Faculdade de Engenharia Química da Universidade Estadual de Campinas como requisito exigido para obtenção do título de Doutora em Engenharia Química.

Supervisor/*Orientador*: PROFESSOR DR. GUSTAVO DOUBEK
Co-supervisor/*Coorientadora*: DRA. CRISTIANE BARBIERI RODELLA

ESTE EXEMPLAR CORRESPONDE À VERSÃO FINAL DE TESE DEFENDIDA PELA ALUNA LETICIA FRIGERIO CREMASCO E ORIENTADA PELO PROF. DR. GUSTAVO DOUBEK.

CAMPINAS

2021

Folha de Aprovação da Defesa de Doutorado da aluna **Leticia Frigerio Cremasco** - RA: 162754 e aprovada em 26 de março de 2021 pela comissão examinadora da defesa constituída pelos doutores:

Prof. Dr. Gustavo Doubek - Presidente e Orientador
FEQ / UNICAMP

Prof. Dr. Ambrosio Florêncio de Almeida Neto
FEQ / UNICAMP
Videoconferência

Dr. Renato Garcia de Freitas Sobrinho
Universidade Federal de Mato Grosso
Videoconferência

Dra. Flavia Regina Estrada
Laboratório Nacional Luz Síncroton - LNLS
Videoconferência

Dra. Elisabete Inacio Santiago
Instituto de Pesquisas Energéticas e Nucleares - IPEN
Videoconferência

A Ata de defesa com as respectivas assinaturas dos membros encontra-se no SIGA/Sistema de Fluxo de Tese e na Secretaria do Programa da Unidade.

Acknowledgements

Before all, I would like to thank my family. My parents Janir and Neide, for the never-ending love and support, for always supporting my decisions and my passions in life. My sister Emilia, for being my first partner and biggest inspiration, even being the little one. My partner Daniel, for being by my side in every bad and great day through this journey, making me feel more loved every new day. Because of you all, life fells lighter and meaningful, and I am eternally grateful.

I am also thankful to my supervisors. Gustavo Doubek for welcoming me in the very beginning of his lab and for believing in me during all my journey in the academic life, for all the orientation and motivation to keep up with the focus when things did not seem to work well. Cristiane Rodella, for opening the doors of the synchrotron universe for me and my group, for deeply believing and supporting the project since the beginning and for teaching always in the most patient way.

I especially thank all the amazing people that crossed my path during these past 4 years. To my lab-mates, Lorrane, Thayane, Chayene, Bianca, sharing life with you has made the challenges easier to surpass, everyday more fun and full of learnings. I am deeply grateful and wish to have the grace of your friendship for all the years to come.

Huge thanks also for all and each the essential Unicamp, FEQ and CNPEM - specially the teams from LNLS, from the beamlines XPD and IR1, and from the *Prédio Vermelho* - employees that somehow helped me during the activities performed to accomplish this work.

My gratitude also goes to the University of Campinas. All the experiences that I had the opportunity to live here have transformed me as a person, and I like better the person I became after this journey here.

Thanks are also due to Conselho Nacional de Desenvolvimento Científico e Tecnológico (CNPq) for the financial support (Grant 140937/2017-0). This work was also supported by FAPESP grant 2017/11958-1, Shell, and the strategic importance of the support given by ANP (Brazil's National Oil, Natural Gas and Biofuels Agency) through the R&D levy regulations.

I also would like to thank the committee members who spent their time to evaluate and contribute to this doctoral thesis.

“A ship in harbor is safe, but that is not what ships are built for”

John A. Shedd.

Abstract

The replacement of fossil fuel-based energy sources and storage systems to renewable ones has increased the interest in high energy density batteries. Lithium-O_2 cells have been drawing researchers' efforts for showing a specific energy density around three times greater than the current batteries in such a way that it can be compared even to the fossil fuels energy density. In a simple way, Li- O_2 devices store electric energy by the formation and decomposition of oxides derived from the reaction between lithium and oxygen. The oxidation of the solid Li_2O_2 that deposits in the cathode pores during discharge is one of the biggest challenges of the system operation, due to the lack of direct electrochemical contact between the catalyst species and the whole extension of Li_2O_2 mass distributed on the electrode surface. In this area, redox mediators (RMs) have been studied as a viable option, because it allows the charge transfer process to take place on the liquid phase during the formation and oxidation of Li_2O_2. However, there is still no scientific consensus that allows the elaboration of a robust project for the system and that results from a lack of knowledge regarding the complex phenomena that happens during this cell cycling, such as catalysis, ion transport and diffusion. In this context, the research projects that culminated in this thesis focused on performing a combination of electrochemical measurements with spectroscopy methods, *in situ* techniques (specifically FTIR and XRD) in order to have a better understanding of these processes and walk towards the development of a prototype for the Li-O_2 batteries. Results presented here show micro and nanoscale FTIR being applied for the first time in this type of system, providing valuable information about the formation of discharge products and electrolyte degradation. *Operando* XRD data shown bring to light how LiBr and LiI, as redox mediators, affect on the dynamic of the cell, reaction routes and kinetics and how the use of these class of material in cells with high loading electrodes can result in moving the issue from catalytic to mass transfer.

Keywords: batteries, lithium-O_2, *in situ* characterization, redox mediators, synchrotron XRD, metal-O_2

Resumo

A substituição de fontes de energia e sistemas de armazenamento baseados em combustíveis fósseis por alternativas renováveis tem aumentado o interesse por baterias de alta densidade energética. Células de lítio-O_2 tem atraído esforços da comunidade científica por apresentar uma densidade energética específica cerca de três vezes maior do que as atuais baterias de lítio-íon, de modo que podem ser comparadas à gasolina em termos de armazenamento de energia. De maneira simplificada, dispositivos Li-O_2 armazenam energia elétrica pela formação e decomposição de espécies oxidadas formadas pela reação entre lítio e oxigênio. A oxidação do Li_2O_2 sólido depositado no cátodo durante a descarga da célula é um dos maiores desafios da para operação da célula, devido a falta de contato superficial direto entre as espécies catalisadoras e a extensão da massa de peróxido de lítio distribuída na superfície do eletrodo. Em relação à essa problemática, os mediadores redox têm sido apresentados como uma opção viável, uma vez que esses compostos permitem que o processo de transferência de carga aconteça na fase líquida, durante a formação e oxidação do Li_2O_2. Entretanto, ainda não há consenso científico para a elaboração de um projeto robusto para o sistema, em decorrência de uma insuficiência de conhecimentos acerca dos complexos fenômenos envolvidos na ciclagem da bateria, como catálise, transporte iônico, difusão. Nesse contexto, os projetos de pesquisa que culminarem nessa tese tiveram foco na realização de uma combinação de medidas eletroquímicas com métodos espectroscópicos e técnicas *in situ* (especialmente FTIR e DRX) de modo a ter um entendimento mais claro acerca desses processos. Os resultados apresentados aqui mostram técnicas de FTIR em micro e nano escalas sendo usadas pela primeira vez nesse tipo de sistema, fornecendo informações valiosas sobre a formação de produtos de descarga e degradação de eletrólito. Dados de DRX *in situ* apresentados esclarecem como LiBr e LiI, como mediadores redox, influenciam na dinâmica da célula, nas rotas e cinética de reação, e como utilizar essa classe de compostos em dispositivos com eletrodos de altas massas de material ativo podem resultar em mudar a problemática de catalítica para transferência de massa.

Palavras-chave: baterias, lítio-O_2, caracterização *in situ*, mediadores redox, DRX sincrotron, metal-O_2

List of Figures

List of Tables

List of Abbreviations

$GtCO_2$	Billion tons of CO_2
GHG	Green house gases
Toe	Tonnes of oil equivalent
EIA	Energy International Agency
XRD	X-ray diffraction
XPD	Name of the LNLS X-ray powder diffraction beamline
SEM	Scanning electron microscope
FTIR	Fourier-transformed infrared spectroscopy
MWCNT	Multi-walled carbon nanotubes
CNPEM	Centro Nacional de Pesquisa em Energia e Materiais Brazilian Center for Research in Energy and Materials
CNT	Carbon nanotubes
CVD	Chemical vapor deposition
LNLS	Laboratório Nacioanl de Luz Síncrotron Brazilian Syncrotron Light Laboratory
LNNano	Laboratório Nacional de Nanotecnologia Brazilian Nanotechnology National Laboratory
OCP	Open circuit potential
RM	Redox mediator
IR	Infrared
IR1	Name of the LNLS infrared beamline
FC	Floating catalyst
DN	Donor number
CINE	Center for Innovation on New Energies Centro de Inovações em Novas Energias
wt	weight
sccm	Standard cubic centimeters per minute
RDE	Rotating disc electrode
SS	Stainless steel
PCs	Pseudocapacitors
DME	Dimethoxyethane

MeCN	Acetonitrile
TEGDME	Tetraethylene glycol ether
DMSO	Dimethyl sulfoxide
SEI	Solid-electrolyte interface
RE	Renewable energy
SERS	Surface enhanced Raman Spectroscopy
XRPD	X-Ray powder diffraction

List of Symbols

η	Overpotential
i	Electrical current
U_0	Standard redox potential
d	Diameter
i_p	Peak current
E_p	Peak potential
A	Electrode area
C_0^*	Initial surface concentration
D_0	Diffusion coefficient
υ	scan rate
E_λ	Switching potential
E_0'	Formal potential of an electrode
η_{cha}	Charge overpotential
η_{dis}	Discharge overpotential
Ω	Mechanical frequency
A'	Amplitude
n	Chemical species valence
F	Faraday's Constant
R	Gas constant
T	Temperature
K	Reaction's equilibrium constant
L	Unit, litres
µ	Unit prefix in the metric system denoting a factor of 10^{-6}
s	Unit, seconds
h	Unit, hours
m	Unit, meters Unit prefix in the metric system denoting a factor of 10^{-3}
n	Unit prefix in the metric system denoting a factor of 10^{-9}
M	Unit, mol/L
V	Unit, J/C (joule per coulomb)

Contents

CHAPTER 1

Introduction

1. Introduction

1.1 Thesis scope and structure

This thesis reports the work developed on the four years between March, 2017 and February 2021. The focus of the work has always been the answers that *in situ* and *operando* characterization of non-aqueous Lithium-O_2 (in this work most referred as Li-O_2) cells would add to issues still unknown regarding this system. After some time, came up the interest in studying the effect of the redox mediators' addition in the system, motivated mostly by the fact that, at that time, there was no published paper demonstrating the redox mediator in time-resolved characterization of Li-O_2 batteries.

The thesis is divided into 6 main chapters.

This chapter, Chapter 1, introduces the thesis, presenting the contextualization and motivation for this study; the objectives and the scientific production developed to date, as submitted and accepted publications.

Chapter 2 consists of the literature review, covering the energy panorama in Brazil and worldwide; an introduction to the Li-O_2 system; topics regarding the electrochemistry of the cell and an overview on the components of the battery that most influence this study.

Chapter 3 covers most of the theoretical background that underlies the topics that integrate this research project, including batteries' introductory information, electrochemistry concepts and techniques, and the fundamentals of the characterization techniques most used in this work.

Chapters from 4 to 6 describe the results obtained for this project, that have resulted in two submitted papers, two conference presentations, both international, and one accepted full paper in congress proceedings (COBEQ 2020).

1.2 Contextualization and motivation

The energy matrixes worldwide rely heavily on fossil fuels to supply the energy demand. Even with the growing political efforts, a change in world's energy system is a slow process (EDENHOFER et al., 2014). In terms of energy utilization, the International Energy Agency (IEA) indicates that in Brazil and also worldwide, the largest energy consumer (total final consumption) has been the transportation sector and the

industry. Regarding green house gases (GHGs) emissions resulting from the energy sector, electricity and heat production and transportation dominate global numbers, followed by the industry (EIA, 2019).

Moving primary energy sources from fossil fuel based to renewable ones is an important and necessary ongoing mission that has been based on the development of new technologies for energy source and storage. As renewables increase its share on power matrixes, intermittent energy source balancing becomes critical and tools for the stabilization of future power grids necessary (IPCC, 2014). In addition, with transports being one of the main GHGs emitters, the transportation sector becomes a relevant segment on the pathway towards insertion of new technologies and fuels in the market. These two factors indicate rechargeable batteries as key elements to promote proper energy management and distribution, since stationary energy storage and electrical vehicles are applications where these devices would play an important role.

In this field, lithium-ion batteries have been the best alternative, however, even after decades of continuous improvement and its wide use in portable devices, the batteries themselves are indicated as the main technological barrier for the large-scale adoption of electric propulsion and battery energy storage systems (BESS). In the case of electric and hybrid vehicles, the relatively low specific energy density provided by the Li-ion batteries causes the current to deliver a limited range (GIRISHKUMAR et al., 2010; PARK et al., 2012). Moreover, when it comes to Li-ion BESS units, the lack of fast response of the units to peak-loads may still make the system susceptible to intermittencies (FAUNCE et al., 2018).

In this scenario, lithium-air batteries has attracted researchers' attention for being a system with potential to provide a specific energy density around three times higher than current lithium-ion cells (LU et al., 2010b), capacity comparable even with fossil fuels like gasoline (GIRISHKUMAR et al., 2010; IMANISHI; LUNTZ; BRUCE, 2014).

Lithium-air or Lithium-O_2 batteries are devices that store electric energy by the formation and decomposition of the product formed by the reaction between lithium and oxygen. During the discharge process, metallic lithium located in anode is oxidized forming Li^+ ions, which are then conducted through the electrolyte to the cathode, where the reaction with oxygen occurs. The process is reversed during charge, releasing oxygen (ABRAHAM; JIANG, 1996; BRUCE et al., 2012; IMANISHI; LUNTZ; BRUCE, 2014).

Among the multiple technological barriers of the aprotic Li-air system, the high potential required for oxidation of the non-conductive and insoluble Li_2O_2, the discharge product, is identified as probably the most challenging one. This high charge overpotential promotes side reactions, such as electrolyte and electrode degradation, which leads to low cyclability and low energy efficiency. In order to overcome this issue, a more efficient oxidation of Li_2O_2 must be promoted (PARK et al., 2018). The use of redox mediators (RMs) has been studied as one viable option. This class of compound is basically a soluble catalyst that is dissolved in the electrolyte and participate in the reaction as an energy carrier. During the RM-assisted charge the mediator is electrochemically oxidized and subsequently oxidizes Li_2O_2 chemically (KO et al., 2019a). The transformation of the charge reaction from electrochemical to chemical, reduces the formation of highly reactive intermediates upon electro-oxidation of lithium peroxide, and reduces the charge overpotential (PARK et al., 2018).

Even after some progress and new interesting alternatives to overcome some of the multiple technological barriers, until the present moment, there is no scientific consensus that allows the elaboration of a robust project for the system. This is mainly due to the still scarce detailed knowledge about the mechanisms involved in the processes, such as surface reaction, ion transport, catalysis and gas diffusion. The combination of electrochemical measurements with spectroscopy methods, *in situ* techniques and the integration of multiple characterizations (Raman, XPS, XRD, FTIR) is crucial towards a better understanding of these mechanisms (FENG; HE; ZHOU, 2016). *Operando* characterization methods are important tools in the process of explaining some scientific issues regarding Li-O_2 technology and providing a direction to future prospective (MA et al., 2016). These time-resolved experiments allow us to understand deeply the reactions, when and how fast they occur, and how variables such as current density, atmosphere influence the system.

1.3 Objectives

This research project focus on the cathode of Li-O_2 battery system with non-aqueous electrolyte. The aim of the project was to investigate deeply the processes that occur in Li-O_2 cells by applying o*perando* and/or *in situ* characterization techniques, XRD and FTIR. A functional carbon material, carbon nanotubes, was used to build electrodes

for the batteries. Allied with cycling, *in situ* characterization allowed a better understanding about the limitations to reaction kinetics or mass transport in the system.

1.3.1 Specific objectives:

- Design cells for *in situ/operando* synchrotron XRD and FTIR characterization;
- Build gas diffusion electrodes using carbon nanotubes;
- Characterize the electrodes *in situ* and/or *operando*;
- Study the redox mediators' effect on the Li-O_2 system using chronopotentiometry.

1.4 Scientific production

The scientific productions developed to date and their status are presented as follows.

Publication I

Title: Baterias Li-O_2 e a influência de estruturas catalíticas ao eletrodo de oxigênio

Authors: Gustavo Doubek; **Leticia Frigerio Cremasco**; André Navarro de Miranda; Lorrane Cristina Cardozo Bonfim Oliveira

Publication type: book chapter **published** - Editora Atena

DOI: 10.22533/at.ed.30919160420

Publication II

Title: Study of the aging process of nanostructured porous carbon-based electrodes in electrochemical capacitors filled with aqueous or organic electrolytes

Authors: Willian G. Nunes, Bruno M. Pires, Francisca E. R. De Oliveira, Aline M. P. de Marque, **Leticia F. Cremasco**, Rafael Vicentini, Gustavo Doubek, Leonardo M. Da Silva, Hudson Zanin.

Publication type: Journal article **published** in the Journal of Energy Storage

DOI: 10.1016/j.est.2020.101249

Publication III

Title: *Operando* Synchrotron XRD of Bromide Mediated Li-O_2 Battery.

Authors: Leticia F. Cremasco, Chayene G. Anchieta, Thayane C. M. Nepel, André N. Miranda, Bianca P. Souza, Cristiane Barbieri Rodella, Rubens M. Filho, Gustavo Doubek.

Publication type: Journal article **published** in the journal ACS Applied Materials & Interfaces.

DOI: 10.1021/acsami.0c21791

Publication IV

Title: *In Situ* Infrared Micro and Nanospectroscopy for Discharge Chemical Composition Investigation of Non-aqueous Lithium-Air Cells

Authors: Thayane C. M. Nepel, Chayene G. Anchieta, **Leticia F. Cremasco**, Bianca P. Souza, André N. Miranda, Lorrane C. C. B. Oliveira, Bruno A.B. Francisco, Julia P. Oliveira, Francisco C.B. Maia, Raul O. Freitas, Cristiane B. Rodella, Rubens M. Filho, Gustavo Doubek

Publication type: Journal article **under review** in the journal Advanced Energy Materials.

Conference presentation I

Title: *In Situ* Nano-FTIR Characterization of Non-Aqueous Lithium-O_2 Cells

Authors: Leticia F. Cremasco, André N. de Miranda, Chayene G. Anchieta, Lorrane C. C. B. Oliveira, Julia P. de Oliveira Julio, Bruno A. B. Francisco, Cristiane B. Rodella, Gustavo Doubek.

Conference: 10^{th} International Workshop on Infrared Microscopy and Spectroscopy with Accelerator Based Sources (WIRMS) - Ubatuba, Brazil, 2019.

Presentation type: poster

Conference presentation II

Title: Lithium Halide as Charge Redox Mediator for Lithium-O_2 Batteries

Authors: Leticia F. Cremasco, André N. de Miranda, Cristiane B. Rodella, Gustavo Doubek.

Conference: Next Generation Materials for Energy Applications – Xiamen, China, 2019

Presentation type: poster

Patent

Patent Invention Request deposited at the Instituto Nacional de Propriedade Industrial (INPI).

Title: Dispositivo Eletroquímico Para Caracterização De Eletrodos Em Regime Dinâmico De Operação

Inventors: André Navarro De Miranda, Gustavo Doubek, **Leticia Frigerio Cremasco**, Thayane Carpanedo De Morais Nepel, Chayene Gonçalves Anchieta e Rubens Maciel Filho.

Deposit date: 21/12/2020

Status: Patent of Invention requested.

CHAPTER 2

Literature Review

2. Literature Review

This literature review focuses on the Lithium-O_2 technology and on its components that most influence this study. Since this topic is very broad and has multiple details, features such as anode, electrolyte and solid catalysts, which are not directly investigated in this study, will not be approached in-depth.

2.1 Energy Panorama

World's dependence on fossil fuels has led to the emission of 1100 $GtCO_2$ in the atmosphere since the XIX century. Table 1 shows data concerning the distribution of primary energy sources in Brazil and globally, classifying them into renewable and non renewable.

Table 1: Primary energy sources distribution in Brazil and in the world in 2017. Source EIA website

Primary energy source				Brazil	Globe
Total, billions of toe*				0.287	13.970
Energy sources	Non renewable	Fossil	Petroleum	38.6%	31.8%
			Natural gas	11.3%	22,2%
			Coal	5.8%	27.1%
		Nuclear		1.4%	4.9%
	Subtotal			57.2%	86.1%
	Renewable	Conventional	Hydro	11.1%	2.5%
		Modern	Renewable fuels	30.1%	9.5%
			Geothermal, solar, wind, thermal, photovoltaic	1.6%	1.8%
	Subtotal			42.8%	13.9%

* toe: tonnes of oil equivalent

The share that corresponds to non renewable energy sources prevails, especially in the global scene where it answers to more than 85% from the total. From this category, the significant majority is based on fossil fuels, both in Brazil and worldwide.

In terms of energy utilization, the Energy International Agency (EIA) indicates that in 2017 Brazilian energy matrix, the largest energy consumer (total final consumption) was the transportation sector (37.2%), followed closely by the industry (34.8%). Globally, transports accounted for 29,0% and industry 28,9%. Regarding GHGs emissions resulting from the energy sector, electricity and heat production and transportation dominate global numbers, reaching 41.4% and 25.5%, respectively (EIA, 2019).

The data emphasize how important and necessary is the development of new technologies for energy source and storage, moving from fossil fuel based to renewable ones. Most countries have been focusing on increasing the share of variable renewable energy (RE) sources such as solar and wind, grid energy matrix. Some are located in geographical regions that favors the large-scale implementation of hydro-power. Some few others have invested in biomass as alternative large-scale energy source (FAUNCE et al., 2018). Based on the data on Table 1, Brazil's matrix has been based on the last two alternatives and regarding the broad participation of renewable sources in the energy base, the country is in a relatively favorable position comparing to most countries in the world. Still, along with the rest of the globe, enormous efforts are yet to be made aiming the development and enhancement of cleaner alternative energy technologies.

As renewables increase its share on power grids, balancing the intermittent energy source becomes critical; as capacities continue to increase and costs continue to fall, batteries will play an important role in integrating renewables and stabilizing future power grids (IPCC, 2014). As transport is one of the main GHGs emitters, the transportation sector becomes a relevant segment on the pathway towards insertion of new technologies and fuels in the market. Current alternatives include the use of hydrogen as fuel, the "dieselisation" of the fleet and the hybridization/electrification of the vehicles (EPE, 2014). This energy transition is now vital and imperative and as a consequence smart grids (that integrate demand response with supplies) and a variety of energy storage solutions are becoming key elements to promote proper energy management and distribution (FAUNCE et al., 2018).

Stationary energy storage and electrical vehicles are two applications that have recently highlighted the rechargeable batteries and increased the interest and motivation on the development of reliable ones (RINALDI et al., 2015).

2.2 Introduction to Li-O_2 Batteries

In order to have a battery with an energy density comparable with fossil fuels a practical gravimetric capacity of approximately 700 Wh kg^{-1} would be necessary (WANG, 1999; WAGNER; LAKSHMANAN; MATHIAS, 2010; BRUCE et al., 2012; IMANISHI; LUNTZ; BRUCE, 2014). Improvements in lithium-ion technologies in the last decades resulted in an increase in its gravimetric capacity to about 250 Wh kg^{-1} (BRUCE et al., 2012). Therefore, the growing interest on the Li-O_2 technology relies on the fact that its gravimetric energy is substantially higher than Li-ion's battery, and can reach values that can be compared even to gasoline. Figure 1 shows a graph that compares several battery systems energy densities with gasoline.

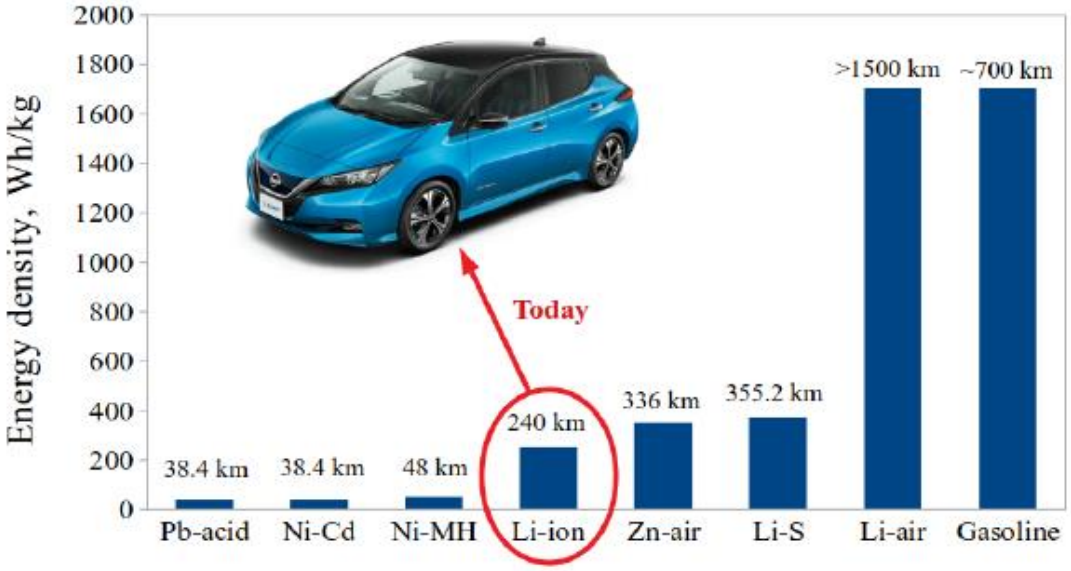

Figure 1: Gravimetric energy density for various battery systems comparing to gasoline. Source: FIATES, 2020.

The Li-O_2 system combines operational elements from the fuel cells (reduction of gaseous oxygen from the environment during discharge) with elements from the conventional batteries (electrons storage and Li^+ ions in a solid phase, Li_2O_2) (GIRISHKUMAR et al., 2010; SHAO et al., 2012). In a simple way, aprotic Li- O_2 cells are devices that store electrical energy produced by the formation and decomposition of products of the reaction between lithium and oxygen (GIRISHKUMAR et al., 2010).

Energy sources based on the metal-oxygen combination are special because oxygen is not stored inside the cell but captured from the environment. The battery anode

consists of a thin metallic lithium foil, which is oxidized to Li^+ ions and conducted by the electrolyte to the cathode, where the reaction with oxygen occurs. During discharge oxygen molecules enter the system through the porous cathode, are adsorbed by the active surface and react with the lithium ions dispersed in the aprotic liquid phase, forming Li_2O_2. The process is reversed in the charge, when Li_2O_2 is decomposed, releasing oxygen back to the atmosphere and metallic lithium is deposited on the anode (ABRAHAM; JIANG, 1996).

Figure 2 shows the schematic operation of the system described above.

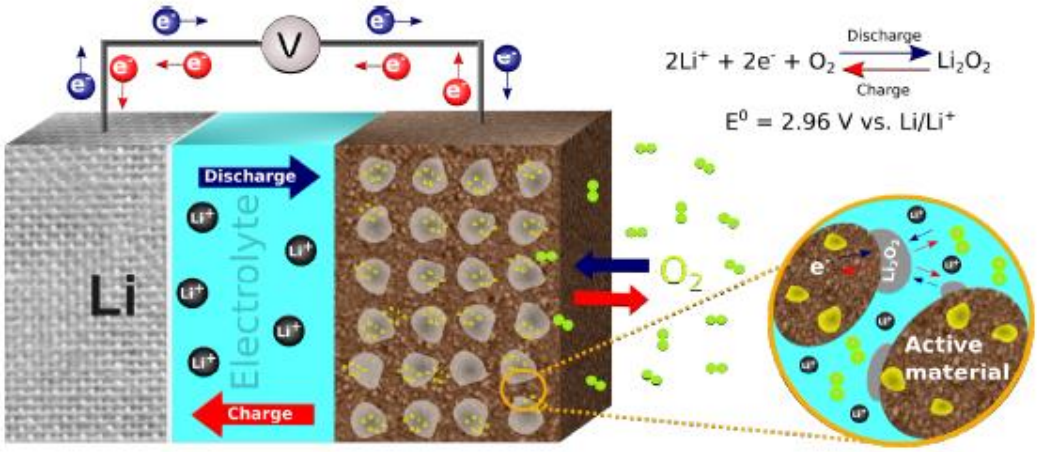

Figure 2: Schematic operation of Li-O_2 battery. Source: FIATES, 2020.

The main technological challenges for Li-air systems are reported as dendritic formation on the lithium metal surface during charging (JO et al., 2011); stability of the electrolyte in the required potential range and in the presence of O_2^- radicals (MA et al., 2015a); effectiveness of the electrode active material or catalyst on reversing the reaction (MITCHELL et al., 2011; CHEN et al., 2013) and its passivation due to the Li_2O_2 formation (LU et al., 2016). The insoluble and nonconductive nature of Li_2O_2, the discharge product expected to be mostly formed, requires the application of a high potential for its oxidation to happen. This high charge overpotential promotes side reactions, such as electrolyte and electrode degradation, which leads to low cyclability and low energy efficiency (LIU et al., 2017b).

2.3 Electrochemistry

2.3.1 Reaction mechanisms

The proposed mechanisms for the fundamental electrochemistry of the lithium-O_2 system are based on the thermodynamics principles for electrochemistry. Table 2 presents the main ones. The first one is expressed in the Equations 1, 2 and 3. The products and intermediate species (Li_2O_2* e LiO_2*) are formed on the surface by the ion transfer process and since these ionic species present almost no solubility in non-aqueous electrolytes they remain deposited in this region (IMANISHI; LUNTZ; BRUCE, 2014)

Beside the mechanisms presented by reactions 2 and 3, others have been proposed. Some authors, for example, suggest that the reaction 2 happens in two steps, with the peroxide being produced through the formation of superoxide, O_2^-, first product of the oxygen reduction with aprotic electrolytes (Equation 4). This anionic radical would react with lithium cations, forming lithium superoxide (Equation 5), a stable intermediate that then, forms lithium peroxide (LU et al., 2010a; FREUNBERGER et al., 2011b) Laoire and coworkers (2010), on the other hand, believe that another reaction would happen to form Li_2O_2, instead of or in parallel, to reaction 2. This reaction is named disproportion and is expressed in reaction 7.

Table 2: Electrochemical reactions proposed for the Li-O_2 system

Discharge	Anode	$2Li \rightarrow 2(Li^+ + e^-)$	(1)
	Cathode	$Li^+ + e^- + O_2^* \rightarrow LiO_2^*$	(2)
		$Li^+ + e^- + LiO_2^* \rightarrow Li_2O_2^*$	(3)
		$O_2 + e^- \rightarrow O_2^-$	(4)
		$O_2^- + Li^+ \rightarrow LiO_2^*$	(5)
		$2LiO_2 \rightarrow Li_2O_2 + O_2$	(6)
Charge		$Li_2O_2 \rightarrow 2Li + O_2$	(7)

* adsorbed species identified on the surface

For the charge process the lithium peroxide can be decomposed by applying an external potential, being the metallic lithium deposited in the anode and O_2 regenerated

in the cathode (GIRISHKUMAR et al., 2010). The charge mechanism is not the inverse of the discharge. Actually, the charge process is believed to occur by a direct reaction with $2e^-$ (Equation 7).

2.3.2 Overpotentials

The standard redox potential of the discharge reaction is $U_0 = 2.96\,V$, indicated in Figure 3 by the dashed line. In this specific case, the open circuit potential (OCP) of the cell is ~3.3 V, significantly higher than U_0. This difference is likely due to the concentration of the species in the system, since this potential is given by Nernst Equation (Equation 8), which is dependent of these concentrations.

$$U = U_0 - \frac{RT}{nF} lnK \tag{8}$$

being n the chemical species valence, F the Faraday's Constant, R the gas constant, T the temperature and K the reaction's equilibrium constant.

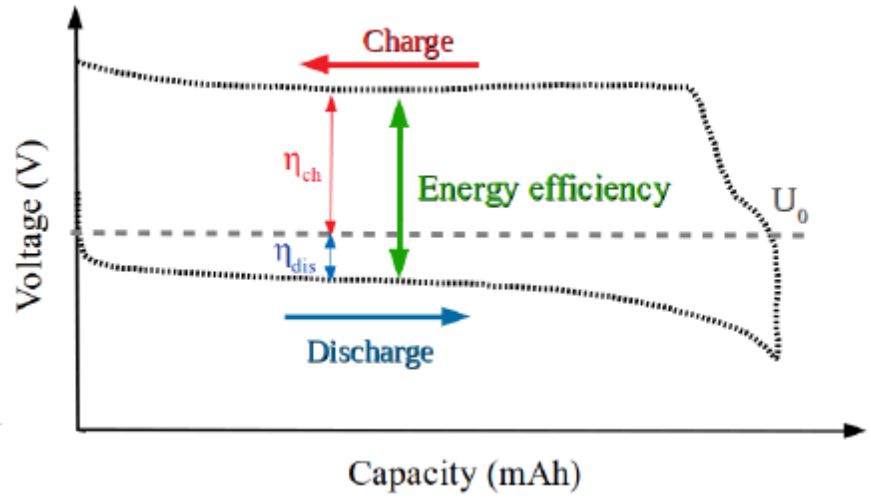

Figure 3: Typical Li-O_2 cell discharge-charge cycle. Source: FIATES, 2020.

The working potential of the cell during discharge is approximately 2.6-2.7 V, lower than U_0. This difference between the standard and discharge working potentials is called discharge overpotential, η_{dis}. During charge the potential increases, with the working voltage around 4.0 V. Analogously, the difference between U_0 and the working

potential of the charge is the charge overpotential, η_{cha}. Based on these values we verify that η_{cha} is higher than η_{dis} (GIRISHKUMAR et al., 2010). These differences occur because in the presence of an electric current the electrochemical system is out of the equilibrium state, and in this state the electrodes potentials, U, are different from the equilibrium values (TICIANELLI E GONZALEZ, 2005).

The deviation from the standard potential increases with the current flowing through the system, and it is named polarization. The deviation is due to the three electrochemical process phenomena that involve the cathodic reaction: reactant approach to the electrode surface, electron transfer reaction and migratory process for compensation of the charge injected in the solution. Depending on the operating conditions of the cell, the effect of one of these steps overlaps to the others (TICIANELLI E GONZALEZ, 2005).

2.4 Cathode structure, materials and solid catalysts

Among the challenges presented on the Introduction to Li-O_2 section (4.2), the oxygen reduction reaction (ORR), that takes place in the cathode, is frequently indicated as the most crucial one. That is because the ORR rate is substantially slower than the lithium oxidation that happens in the anode, dominating the overall rate of the discharge-charge processes. For this reason most Li-air research focuses on the cathode and not on the anode (ZHANG; FOSTER; READ, 2010; MA et al., 2015b).

The electrode's material and architecture impact significantly on the Li-O_2 battery performance (XIAO et al., 2010, 2011), being the cell's storage capacity strongly influenced by the O_2 cathode (BEATTIE; MANOLESCU; BLAIR, 2009; ZHANG; FOSTER; READ, 2010). Since the discharge reaction products are insoluble in the aprotic electrolytes and remain deposited on the cathode, it is necessary that the electrode has a proper porous structure to ensure cell's recharge capability (LAOIRE et al., 2010). Figure 4 shows a schematic representation of the porous gas diffusion electrode and a proposed chemistry on its surface. The capacity that a Li-air battery can reach depends on the carbon microstructure, which includes the superficial area, the pore size distribution and the pore volume. An optimized microstructure not only increases site accessibility but also provides a shorter path for oxygen transfer (PARK et al., 2012).

According to Zheng and co-workers (2011) pores in the micro range have their inlets quickly blocked by the electrolyte or by the produced Li_2O_2 hindering future access into the electrode structure. Macropores on the other hand are easily soaked by the electrolyte, minimizing the triple junctions necessary for the reaction to happen. Therefore, the discharge capacity would be determined by mesopores. (ZHENG et al., 2011).

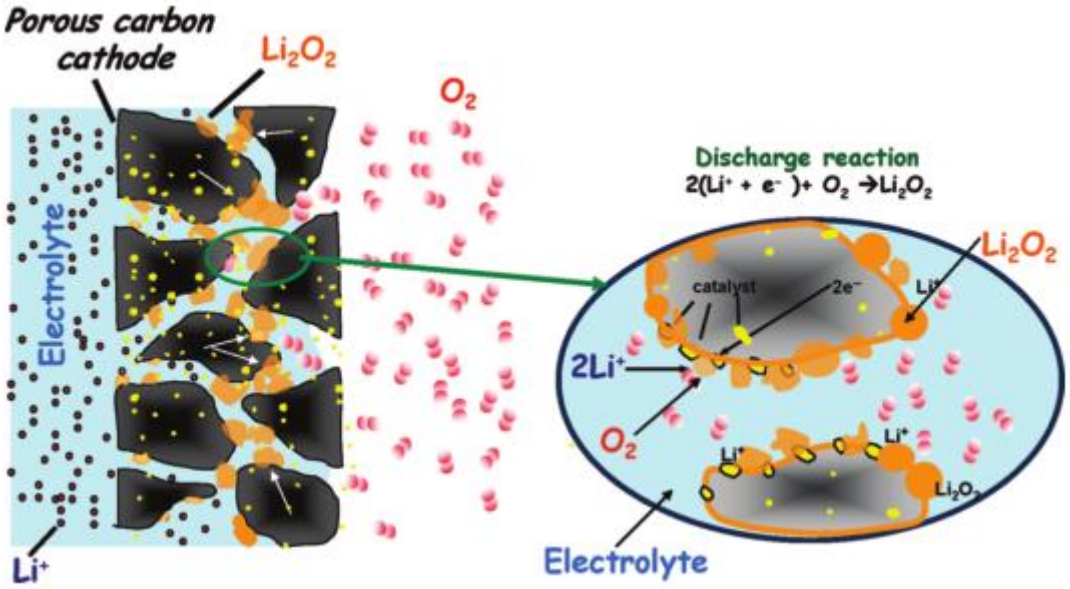

Figure 4: Schematic representation of the porous gas diffusion electrode and a proposed chemistry on its surface. Source: Girishkumar et al., 2010.

At the current scenario of Li-O_2 technology, commercial, functional and N-doped carbon materials are the most used to build the porous cathode. The oxidation of the solid Li_2O_2 that deposits in the cathode pores during discharge requires high overpotentials, risking both the stability of the cathode material and the electrolyte solution. Besides being insoluble, the Li-peroxide is an insulating compound that increases the electron transfer resistance in the system, increasing charge overpotential and reducing the efficiency of the cell. In order to improve the energy efficiency and reduce components decomposition, many approaches have been investigated, changing cathode structure and composition, assessment of multiple electrolyte solutions stability, use of several classes of catalysts.

Among these approaches, the use of catalysts that facilitates ORR and specially OER kinetics has been shown as the most effective. Precious metals and/or their oxides and transition metal oxides are combined with the cathode matrix to operate as

catalysts to the system improve the overall performance of the cells (MA et al., 2015). It has been shown that the use of catalysts, reduce ORR and OER overpotentials and increase the cell's roundtrip efficiency (LU et al., 2010b). The effect of catalyst use can be seen in Figure 5, that illustrate the results obtained by Lu et al (2010c), who developed a highly active bifunctional electrocatalyst using Pt and Au nanoparticles loaded into carbon (Vulcan), significantly reducing both discharge (Au) and charge (Pt) reactions overpotentials.

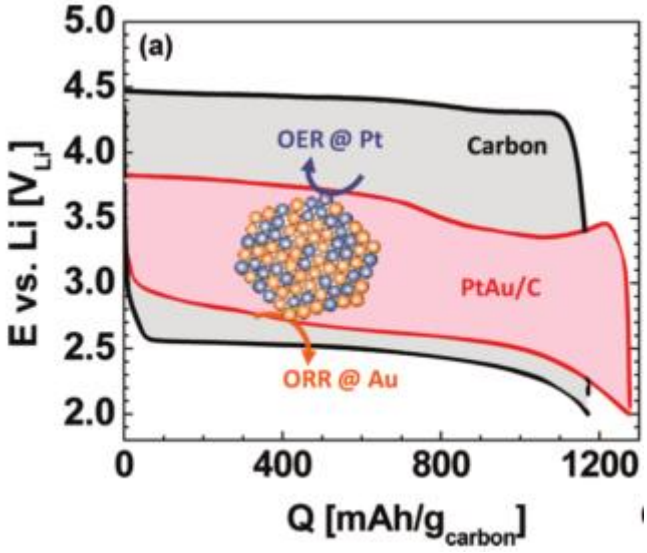

Figure 5: Cycling profile of Li-O_2 cell with and without the use of catalyst. Source: Lu et al., 2010b).

2.5 Redox Mediators

Studies with solid catalysts show significant improvement on the cells' performance, however, the use of these traditional catalysts in an efficient way is very challenging. That is because the interaction between the catalyst particles at the electrode surface and the insulating lithium peroxide deposited on the cathode are hampered by the lack of direct electrochemical contact between the catalyst species and the whole extension of Li_2O_2 mass distributed on the surface (PARK et al., 2018).

In this context, recent studies regarding the use of a class of compound called redox mediators (RMs) has been studied as a viable option for enhancing the system performance. These are compounds that, added to the electrolyte solutions, act on the ORR and OER due to its property of accepting and donating electrons, reversely, at a

known potential. It is an interesting concept for the Li-O_2 system because it allows the charge transfer process to take place on the liquid phase during the formation and oxidation of Li_2O_2 (MCCLOSKEY; ADDISON, 2017). In other words, these are basically soluble catalysts that are dissolved in the electrolyte and participate on the reaction as energy carrier. During the RM-assisted charge the mediator is electrochemically oxidized (Equation 9) and subsequently oxidizes Li_2O_2 chemically (reactions of Equations 10, 11 and 12) (PARK et al., 2018; KO et al., 2019b). The transformation of the charge reaction from electrochemical to chemical, reduces the formation of highly reactive intermediates upon electro-oxidation of lithium peroxide, and reduces the charge overpotential (PARK et al., 2018). Figure 6 is a schematic image that shows how RMs act, comparing to the conventional solid catalysts.

$$RM \rightarrow RM^{ox} + e^- \quad (9)$$

$$Li_2O_2 + RM^{ox} \rightarrow LiO_2 + RM + Li^+ \quad (10)$$

$$LiO_2 + RM^{ox} \rightarrow O_2 + RM + Li^+ \quad (11)$$

$$Li_2O_2 + RM^{ox} \rightarrow O_2 + RM + Li^+ \quad (12)$$

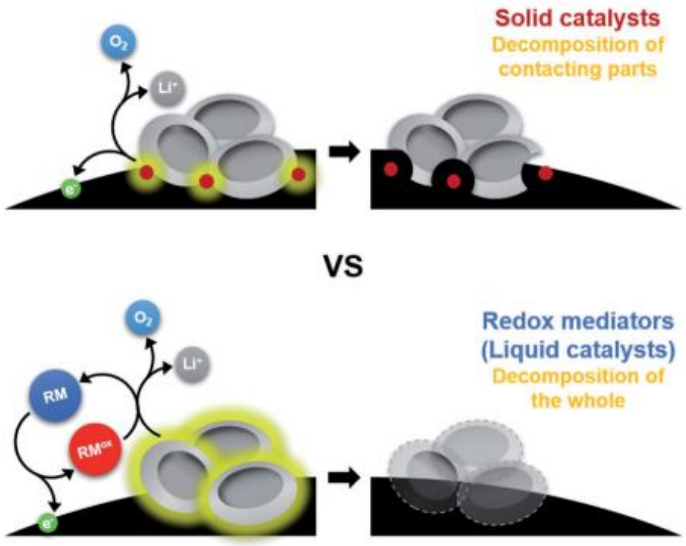

Figure 6: Schematic image for Li_2O_2 decomposition during charge with solid catalyst (upper) and redox mediators as liquid catalysts (lower). Large grey particles are the insoluble discharge products and the small red dots are solid catalysts. Source: Park et al., 2018.

The RM choice depends on the suitability of the corresponding redox potential to the cell desired charge potential, in such way that parallel reactions can be entirely avoided (PARK et al., 2018). Basically, the majority of the RMs can be classified

into three categories: organic, organometallic and halides. Several important works related to the use of some redox mediator molecules in Li-O_2 system, mostly in these three categories.

Overall, organic RMs have been found to be effective in lowering the charge overpotential and even promoting high specific capacity ORR, however, their use indicates possible reactivity with metallic lithium anode and with the oxygen species formed during ORR (CHEN et al., 2013; QIAO; YE, 2016; GAO et al., 2017).

Organometallic Li-O_2 batteries RMs are based on transition metal cations bounded by coordinative bonds to organic aromatic ligands. The redox potential is mostly influenced by the metal ion. They may influence both OER and ORR, being the effect on OER purely electrochemical. Despite all the interesting properties, similarly to the organic, organometallic RMs can be involved in side reactions with the anode and show some instability on the Li-O_2 system, frequently related to decomposition of ligands, leading to CO_2 evolution (SUN et al., 2014; PARK et al., 2018).

LiI and LiBr are the salts that constitute the halide RMs class. Both involve two redox couples (X^-/X_3^- and X_3^-/X_2) (PARK et al., 2018). Li_2O_2 reacts readily with I_3^- (LIM et al., 2014; KWAK et al., 2015; LIU et al., 2015) and Br_3^- (KWAK et al., 2016; LEE; PARK, 2016; LIANG; LU, 2016; XIN; ITO; KUBO, 2017) to produce O_2, Li^+ and X^-. Due to their non-complex nature, these halides are not potentially reactive with Lithium and oxygen reaction products (PARK et al., 2018).

2.6 *In situ* and *operando* characterization of Li-O_2 batteries

Although Li-O_2 technology has experienced significant progress during the past decade, numerous scientific challenges remain. Understanding these barriers is crucial for the development of efficient and rechargeable cells. In order to have a deeper knowledge regarding the processes that take place in Li-O_2 system, the characterization of the cells has been pointed as the leading pathway (MA et al., 2016).

Some studies have been conducted using *in situ* characterization methods. Lu and co-workers (2013) used X-ray photoelectron spectroscopy (XPS) to characterize cells free of carbon, binder and aprotic electrolyte and show evidence of parasitic reactions between common impurities in air and the products of Li-O_2 reactions. Using the same

cell and technique, they provide evidence of reversible lithium peroxide formation and decomposition *in situ* (LU et al., 2012). Peng and co-workers (2011) present *in situ* surface-enhanced Raman spectroscopy (SERS) data that provide evidence that LiO_2 is indeed an intermediate on oxygen reduction reaction (ORR), which then disproportionates to Li_2O_2. *In situ* infrared spectroscopy (FTIR) was used by Mozhzhukhina et al (2013) to study the stability of dimethyl sulfoxide. They have identified the anodic oxidation of the solvent in the presence of trace water above 4.2 V vs. (Li/Li^+) on gold and 3.5 V on platinum. Ryan and co-workers (2013) used a coin cell with a Kapton window to perform an *in situ* study by synchrotron XRD and have shown the formation of crystalline Li_2O_2 on a plain carbon cathode under normal cycling conditions. A Swagelok cell was used by Shui et al (2013) for an *operando* XRD study of Li reversibility. X-ray patterns were collected while the cell's discharge-charge cycles were carried out. In 2014, Gittleson and coworkers published their work using *operando* surface-enhanced Raman spectroscopy to investigate the cathode interface in $Li–O_2$ batteries during cycling (GITTLESON; RYU; TAYLOR, 2014). Li_2O_2 decomposition in electrodes with Ru/MNT catalysts during galvanostatic and potentiostatic charge processes was assessed by Liu et al (2017a) by *operando* synchrotron XRD. More recently, Virwani and his group (2019) published their results performing in situ AFM visualization of $Li\text{-}O_2$ discharge products.

Most of these briefly mentioned studies, however, use cells configurations such as coin cell, pouch cell or capillary, which are not designs that approach possible future prototype architectures. In addition to that, only one redox-mediated system investigated with an *operando* characterization was found to be reported, which is the study conducted by Li and coworkers (2017), that performed *operando* synchrotron XRD experiments for understanding the electrochemical formation and decomposition of Li_2O_2 and LiOH using LiI as redox mediator.

CHAPTER 3
Theory

3. Theory

This chapter touches on the theoretical background that underlies the topics that integrates this research project.

3.1 Batteries

In a general way, the minimal configuration of a practical electrochemical system comprises two (electrical conductors) electrodes and an electrolyte (ionic conductor). In one of the electrodes, the anode, an oxidation reaction happens, while in the other, the cathode, a reduction reaction takes place. The electrolyte participates on this process by doing the ionic charge transport. When these two reactions happen in two different electrodes that are isolated electrically in such way that the electrons involved are forced to circulate through an external circuit, the energy released from the electrochemical reaction is converted into electric energy. Separators are an important component of these cells, preventing physical contact between the anode and cathode and accordingly, a short-circuit. Meanwhile, they should retain the electrolyte, allow and facilitate the ion transport in the cell (TICIANELLI E GONZALEZ, 2005).

Primary batteries are the classification of electrochemical systems that provide electrical work from reactants contained in its interior, and when these reactants are depleted the system is disposed. The most common representatives of this class of batteries are the ones that consist of Zinc and Manganese dioxide electrodes, Zn/MnO_2, the alkaline battery and the “zinc chloride cell, Zn/Cl” (TICIANELLI E GONZALEZ, 2005).

The essential difference from a primary to secondary battery is that in the last system the reactions responsible for the energy generation can be reversed. After discharge the system can be regenerated and go through a number of cycles, depending on the type of battery. Lead-acid batteries, have been the dominant technology for large-scale rechargeable batteries for a long time. However, their numerous limitations have encouraged the development of novel battery technologies, which led to the Li-ion cells. These are the most significant representant of the secondary batteries and are considered by many the major breakthrough in the area of electrochemical energy storage in recent times (FAUNCE et al., 2018).

3.1.1 Battery configuration

i. Anode

In the case of Li-ion batteries, which weight of the cathode and electrolyte dominates the battery's energy density, anodes with low specific capacity, such as LiC_6 are acceptable. When it comes to Li-O_2 cells, with substantially light cathodes replacing the intercalation cathodes, having a high specific anode capacity becomes relevant (GIRISHKUMAR et al., 2010). Metallic lithium has a very high specific capacity and is currently the most frequently used anode material. Nonetheless, its use as anode is associated with issues, such as dendrites formation and shorts between electrodes.

As lithium is immersed in an organic solvent a passivation layer, known as solid-electrolyte interface (SEI), is formed. The contact between the metal and the solvent promotes a spontaneous and almost immediate reaction that forms a Li-ion conductive film on the surface. As this reaction proceeds its kinetics is inhibited by a multilayer lithium salts deposits that creates a barrier, preventing further metal corrosion (AURBACH, 2000). The SEI is chemically heterogeneous, which can lead to a structure that is morphologically heterogeneous and brittle, favouring defects upon repeated cycling. Such defects can promote uneven current distributions at the SEI resulting in dendrite formation (CHOI et al., 2004).

There are several approaches aiming to reduce dendrite formation during battery cycling, among which are the use of polymeric electrolytes, solid state electrolyte based on ceramic materials or Li-ion conductive glasses or even producing anode alternatives (GIRISHKUMAR et al., 2010). These are very important studies for the Li-O_2 area, however, it is known that the reaction that takes place on the anode is fast and that the Li-O_2 system large overpotentials are associated to some kinetic activation barrier in cathode chemistry (GIRISHKUMAR et al., 2010). For this reason, this study focuses on cathodic reactions and, therefore, anode issues will not be deeply explored here. Metallic lithium was the only material used as anode throughout this study.

ii. Cathode

Despite the challenge that the O_2 presence brings to the anode, the cathodic reactions are the ones that remain mostly unclear, thus are the major object of investigation (IMANISHI; LUNTZ; BRUCE, 2014).

Oxygen solubility and diffusion coefficient are relatively small in organic electrolytes, which make the discharge reaction kinetics slow. At a slow discharge rate the capacity of the cell is limited mainly by the properties of the cathode (YOUNESI, 2012). The effect of carbon materials and other compositions of cathode reaction layers on battery performance has been vastly studied.

Activated carbon, multi-walled carbon nanotubes, fullerenes, graphene are all carbon-based materials well established as interesting options for electrodes application in electrochemical energy storage devices, such as electrical double-layer capacitors (EDLCs) and pseudocapacitors (PCs)), metal air batteries, fuel cells. The success of these materials in electrochemical applications is due to its high electronic conductivity, chemical stability, fast charge-transfer for redox reactions, high surface area, easy synthesis and functionalization, great abundance, and low cost (TO et al., 2015).

The performance of these devices is fundamentally dependent on the capability of the carbon material interacting with ions and transport electrons. For most of these devices the electrode, ideally, should present high conductivity for electron transport, high surface area for effective ion adsorption/ desorption, and suitable pore architecture for rapid access of ions from electrolyte solution to the carbon surface. Regarding these features, some of the carbon materials present drawbacks (TO et al., 2015). Active carbons (ACs), for example, have high large pore tortuosity, poor pore connectivity and presence of high surface concentration of micropores ($d \leq 2$ nm) severely limit electrolyte ion transport to the surface. Graphene, on the other hand, in contact with different electrolytes, leads to a porous structure that hinders the efficient transport of electrons and solvated ions in the active regions of the porous electrode material (TO et al., 2015).

Carbon nanotubes (CNTs) have been attracting increasing interest because of their morphological characteristics that allow the desired charge storage mechanism at the electrode/solution interface to happen (MASARAPU; WEI, 2007). The fabrication of well-designed nanoarchitectures composed of CNTs enables a fine-tuning process accounting for the carbon interaction with the solvated ions, as well as facilitated electron and ion transport across the bulk of the porous carbon material (SZUBZDA; SZMAJA; HALAMA, 2012).

Based on literature review and the results obtained during my Master's project, we verified that, compared to the standard carbon materials (e.g. activated carbon, carbon black, Super P, Ketjen Black), cathodes built with functional carbon delivers better

results. The Carbon Sci-tech lab, that with our laboratory, integrates CINES's Advanced Energy Storage Division, already had a significant knowledge and infrastructure for growing carbon nanotubes (CNTs) by the floating catalyst based chemical vapor deposition method (FC-CVD). For these reasons, this material was chosen to constitute the cathode matrix in most of the research fronts of this project.

iii. Electrolyte

The use of nonaqueous solutions has substantially grown in the sector of modern electrochemical technologies. Among these applications the following can be highlighted: capacitors, primary and secondary lithium batteries, conducting polymers, electrochemiluminescence, electrochemical reduction of CO_2, electrodeposition and others (IZUTSU, 2009).

Regarding the Li-O_2 system four chemical architectures have been proposed, each approach is reasoned on a type of electrolyte used. Three of them are based on liquid electrolytes, an aqueous, an aprotic and a mixed system, with an aqueous electrolyte surrounding the cathode and an organic immersing the anode. The fourth approach, the most recent proposed one, consists of an all-solid-state battery, with a solid electrolyte (GIRISHKUMAR et al., 2010). Each battery configuration has its advantages and brings specific scientific and engineering challenges, but until a recent time the non-aqueous architecture was the only one to show evidence of consistent electrical rechargeability. For this reason, this was the electrolyte category chosen to be used in this study and the theory around electrolytes will only comprise the aprotic solvents.

In a general base, electrolytes must comply with a series of requirements to suit well the Li-O_2 system: sufficiently high **conductivity**; low **volatility**; adequate **O_2 solubility and diffusivity**; ability to promote some **solubility of Li_2O_2**; ability to wet electrode surface and **stability** within the potential window, in contact with O_2 and its reduced species, discharge products such as Li_2O_2 and its intermediates and in contact with the anode or stable SEI formed on the anode (IMANISHI; LUNTZ; BRUCE, 2014).

The chemical nature of the electrolyte is one of the key factors affecting the discharge and charge reaction kinetics, potential and cell cyclability. That is because many aprotic electrolytes exhibit decomposition at the cathode during the aprotic Li-O_2 battery operation (IMANISHI; LUNTZ; BRUCE, 2014). Carbonate-based electrolytes were early found to be decomposed during cycling, forming insoluble Li_2CO_3

(FREUNBERGER et al., 2011a). After that, multiple solvents have been tested: dimethoxyethane (DME), acetonitrile (MeCN), tetraethylene glycol ether (TEGDME), dimethyl sulfoxide (DMSO), ionic liquids (LIU et al., 2017b). Still, there is not a specific one that meets all the demands. Based on results that show evidence that DMSO can be associated with a good cyclability (XU et al., 2012) and enhanced kinetics (GITTLESON et al., 2014), this solvent was selected for this study.

3.2 Electrochemistry

3.2.1 Overpotentials

Electrochemical devices are systems that operate with an external electrical charge connected to it, with a circulating current. With this external charge connected, the potential between the electrodes becomes a function of the current. The displacement of the electrode potential from the equilibrium value is referred to as polarization and its magnitude is larger as the circulating current increases. Its value corresponds to the reversible potential, subtracted of three electrode polarization components, that will be presented here (TICIANELLI E GONZALEZ, 2005).

The origins of the displacement from the equilibrium potential derive from three different electrochemical process phenomena that are involved in a cathodic reaction: approximation of the reactant to the electrode surface, electron transfer reaction and migratory process of charge compensation. Depending on the operating conditions of the cell one of these effects overlaps the others (TICIANELLI E GONZALEZ, 2005):

a. When the reactants concentration is high and/or the current is low, the process kinetics is limited by the electron transfer reaction, making this reaction the rate-limiting step. In this case, the potential displacement is called **activation polarization**.
b. When the electrolyte conductivity is low and/or the concentration of the ions responsible for the charge transfer is low, or still if the current is very high, the solution's electroneutrality is hampered, slowing the process. This phenomenon is guided by the Ohm's law, which why under these conditions the displacement is called **ohmic loss polarization**.

c. When the reactants concentration is low and/or the current density is high, there is a depletion of reagent species on the electrode surface. The speed of arrival of these species to the surface becomes the rate-limiting step and origins of the **mass transfer polarization**.

Each of these potential displacements has a different relation with the current, *i*, that circulates through the system. Figure 7 illustrates graphically how each of the polarizations contributes, as a function of *i*, on the cell's potential.

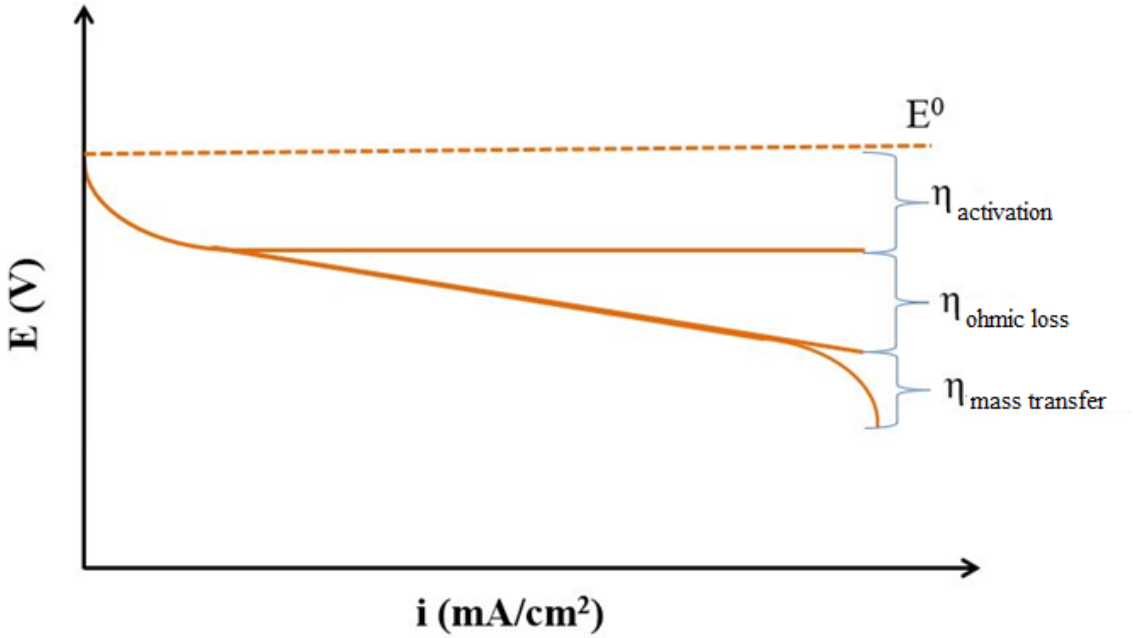

Figure 7: Voltage-current curve of electrochemical cell, showing the types of polarization effects: cell reversible potential, equilibrium value; curve resulting after adding activation polarization; curve resulting after adding the ohmic loss contribution; curving resulting after adding mass transfer polarization. Source: FRANCISCO, 2020.

3.2.2 Galvanostatic Cycling - Battery testing

The galvanostatic cycling is a test used to access the performance and cycle-life of batteries and capacitors. The test consists basically in a loop of constant-current chronopotentiometries, where the applied current signal alternates, being negative while discharging and positive while charging. Each repetitive loop of charging and discharging is called a cycle.

Usually, each cycle part is conducted until a set voltage or time is reached, depending on the interest of the user. The cycle charge, which is commonly referred as capacity, has the unit of ampere-hour (Ah), where 1 Ah = 3600 coulombs.

Qualitatively describing the constant-current chronopotentiometry, the current, i, is applied to the electrode, causing a constant rate reduction of the species on the cathode battery side. The electrode potential varies according to the initial/reduced species couple, as the concentration ratio continuously changes at the electrode surface. After a certain time, the concentration of the initial species drops to zero at the electrode surface and the flux of that species to the surface is no longer enough to accept the totality of the electrons from the electrode-solution interface. At this point the electrode potential changes abruptly until it reaches a second reduction process potential. The shape and position of the described $E - t$ curve depends mostly on the system composition and the rate constant. As the set voltage or time is reached, the current is reversed, changed to an anodic current of the same magnitude. The potential, then, moves to the opposite direction. This charge-discharge pattern can be continuously repeated, stablishing multiple cycles (BARD; FAULKNER, 2000).

In order to be able to compare results with the literature in this field of study it is essential that we normalize the capacity of the battery. The most common normalizations are by electrode area (cm^2) and electrode active material mass (g_c). For each cycling, with the test's length of time (h), the current applied (A), electrode's area (cm^2) and catalyst mass in the electrode (g_c), the discharge and charge capacities of the cell are calculated and cycling profiles are given in graphs E vs. mAh g_c^{-1} or E vs. mAh cm^{-2} as observed in Figures 3 and 5, in the Literature Review chapter (Chapter 2).

3.3 Characterization techniques

This section covers the fundamentals of the characterization techniques employed in this research.

3.3.1 X-Ray Diffraction (XRD)

Powder x-ray diffraction is a technique mainly used to identify polycrystalline materials in a sample and even measure the sample purity. The majority of solid materials is crystalline (minerals, inorganic compounds) and can be characterized by XRD (ATKINS AND JONES, 2006).

A crystalline material consists of a build up of periodic smaller structural units, called crystals. The unit cells, which are the smallest repeated structures in the crystal, are classified into different forms. The relation between the axes lengths (identified as *a, b, c*) and the difference of the angles (identified as α, β, γ) defines the lattice system of the crystal. In the crystal, the ordered atoms are arranged in a 3D setup creating several different planes of atoms in all directions in the crystals. These planes are the lattice planes, which are defined by the Miller index, that used three coordinates to describe the plane, *hkl*.

X-rays have a wavelength that has the approximate range of the distance between atoms in a solid crystal, ~ 10^{-10}, which means that X-ray may interact with an array of atoms. During the operation of the technique, when an X-ray hits an atom of a crystalline sample, it is scattered by the electrons of this atom. If the Braggs's law (Equation 13) is satisfied, an atom from a parallel plane reflects the X-ray in a similar direction, leading to constructive interference.

$$n\lambda = 2dsin\theta \tag{13}$$

In Equation 13, λ is the radiation wavelenght, in Å, n is a whole number, d is the planer lattice spacing, in Å, and θ is the radiation incoming and reflected angle, in degrees.

The diffracted rays produced by the interaction between the incident ray and the atom are detected, processed and counted (ATKINS AND JONES, 2006). The generated x-ray pattern is interpreted by comparison with standard reference pattern, since each crystal structure has its own pattern.

Synchrotron X-ray radiation has higher intensity, higher brightness, better angular resolution, and tuneable wavelength compared to common X-ray sources. This allows experiments with shorter time exposure experiments with good intensity and a localized beam, which is ideal for *in situ* studies of batteries, due to its short-time exposure with good intensity and a localized beam (STORM, 2016). Synchrotron X-ray was used in an important part of this work.

The crystal structure describes the atomic arrangements of the material. Its interatomic distances determine the position of the diffraction peaks and the atom position determines the peaks' intensities (ATKINS AND JONES, 2006).

3.3.2 Fourier-transform infrared spectroscopy (FTIR)

Spectroscopy studies the interaction between the electromagnetic radiation and matter. As the radiation interacts with any material, it can be reflected, absorbed, transmitted or scattered. These interactions can cause modifications in the configuration of the chemical bonds of the material, leading to transitions in the energy levels of the molecules. The spectral region where the transitions are observed depends on the types of levels involved, i.e. electronic, vibrational or rotational. Normally, electronic transitions are located in the ultraviolet or visible regions; vibrational in the infrared region; and rotational in the microwave region (SALA, 2008).

Absorption of infrared (IR) radiation happens when a molecule, as it vibrates and rotates, undergoes a net change in its dipole moment. An electric dipole moment variation is related to the modification on the electrostatic attractions between nucleus and electrons that are caused by the chemical bonds vibrations and produces distortion on the molecules' electrical charges. If the electromagnetic radiation frequency equals the vibration frequency in a molecule, the radiation is absorbed. Some few compounds cannot absorb IR radiation, such as O_2, N_2 and Cl_2, promoting no net change in dipole moment of these species during vibration or rotation (SKOOG; HOLLER; CROUCH, 2006).

IR spectra can be obtained by absorption/transmission or reflection of the radiation on the sample. Usually, for transparent samples absorption/transmission is used, while for opaque samples reflection is applied. The equipment mostly used for IR spectroscopy are the Fourier-Transform Spectrometers. The radiation passes through an interferometer - composed of a beam splitter and two mirrors (one fixed and one mobile), where constructive and destructive interference occurs from the waves that return from the mirrors, producing the interferogram.

In this thesis we applied a FTIR-based technique to characterize the studied system. Scattering scanning near-field optical microscopy (s-SNOM) is a technique that uses light scattering from a sharp metal tip of an atomic force microscopy (AFM), allowing infrared probe with spatial resolution beyond the diffraction limit of light. The s-SNOM allows the identification and characterization of chemical composition with nanometer spatial resolution. It works in semi-contact mode controlling a metallic atomic force microscope tip, in close proximity to the sample, oscillating with amplitude (A') in its fundamental mechanical frequency (Ω). Conventionally, lasers are used as the source

of s-SNOM due their high irradiance, however, the narrow tuning range limits the IR region. Aiming to solve this, a technique that couples s-SNOM with broadband infrared synchrotron radiation, synchrotron infrared nanospectroscopy (SINS), was developed. SINS allows to explore the entire mid-infrared spectra in the nanoscale of samples (KEILMANN; HILLENBRAND, 2004).

Note that the tip-scattered light is broadband since the IR synchrotron excitation is broadband. Thereby, in analogy to conventional IR spectroscopy, SINS spectroscopy is accomplished by interferometry being the interferogram detected by a mercury cadmium telluride detector (MCT, MCT, IR-Associates). The signal from the MCT detector is de-modulated by a lock-in based electronics, having Ω is the driven frequency, delivering the SINS spectra from the high harmonics of Ω. The lock-in based detection allows for the amplitude and phase spectra.

3.3.3 Raman spectroscopy

Raman spectra is obtained from the inelastic scattering of a sample irradiated with a monochromatic visible or near-IR laser source, resulting in the molecule moving from a molecular vibrational state to another one. Both infrared and Raman spectroscopy measure the vibrational motions of a molecule. However, the physical method used for observing these vibrations differs. In Raman spectroscopy light scattering is measured while in infrared is based on absorption of photons (VAN KRANENDONK, 1974). In the Raman effect, activity is related to the dipole moment induced in the molecule by the incident radiation electric field. On the infrared, on the other hand, the variation of the intrinsic dipole moment is considered (SALA, 2008; SMITH; DENT, 2005). Most of the electromagnetic radiation scattered by matter has the same wavelength as the radiation source. That is known as elastic scattering or Rayleigh scattering. A small fraction of the scattered radiation, however, has a frequency different from the incident one, which is known as inelastic scattering or Raman effect (SALA, 2008).

In the scattering process the incident photon promotes change in all energy levels, reaching the so-called “virtual state”, that is not a quantized energy state. In the Rayleigh scattering, the photon collision raises the molecule to the virtual state which then returns to the starting energy level, with the scattered photon without any modifications on its frequency. In Raman Stokes scattering, after the photon-molecule

(with energy $h\nu_{in}$) interaction the molecule terminates at a vibrational level higher in its fundamental energy level; in Raman anti-Stokes, conversely, the final energy level is lower than the starting one (SALA, 2008).

Raman spectroscopy uses the inelastic scattering fundamentals to investigate molecular characteristics. The technique considers that, once energy is conserved during the scattering process, the photon energy difference must correspond to an energy change in the molecule. Thus, measuring the photon's energy loss or gain allows the identification of molecular vibrations, which provides information regarding molecular properties (SMITH; DENT, 2005).

The intensity of Raman peaks related to the concentration of the analyte. It is important to appreciate that the magnitude of Raman shifts is independent of the wavelength of excitation.

3.3.4 Scanning electron microscopy

The scanning electron microscope (SEM) is an instrument that allows the examination and analysis of the microstructure morphology. The technique was based on the discovery that electrons can be defected by the magnetic field and has been developed by the replacement of a light source with a high-energy electron beam (ZHOU et al., 2007).

A focused electron beam hits the sample and the interaction between them produces multiple types of signals, which are detected and are used for image formation. Secondary electrons, backscattered electrons, characteristic X-rays are the main ones used for microstructure analysis (ZHOU et al., 2007).

The beam electron energy and the atomic number of the specimen are the two parameters that determine the size and shape of the so-called region of primary excitation. This is the zone that comprises the distance between the specimen surface and the point where the beam encounters and collides with an atom of the sample. An increase in the beam energy leads to larger penetration depth and volume. Higher atomic number, on the other hand, results in smaller penetration factors, since specimens with higher atomic number have more particles to stop beam penetration. Concerning the influence of these parameters on SEM image, a deep penetration length with a large primary excitation

region result in the loss of detailed information. At higher the accelerating voltage, a lower the image detailing and resolution is usually evidenced (ZHOU et al., 2007).

The signal type mostly used on the technique is the secondary electron emission signal. That is because, for having a low energy (3-5 eV), they scape a few nanometers from the material's surface, thus being more accurate on marking the position of the beam and giving topographic information with good resolution. They are used mainly for topographic contrast of the image, allowing a better visualization of surface texture and roughness. In the case of backscattered electrons, they are used for both compositional and topographic information, providing atomic number contrast in the SEM image. This is defined as the electron that has undergone scattering events and escapes from the surface with an energy greater than 50 eV (ZHOU et al., 2007).

CHAPTER 4

In situ synchrotron micro and nano-FTIR technique for Lithium-O_2 batteries characterization

4. *In situ* synchrotron micro and nano-FTIR technique for Lithium-Air batteries characterization: Publication IV

4.1 Introduction

The current research in the Li-air batteries, with vistas to a successful technology, has their operation in ambient atmosphere as one of the major goals. It is required to deepen the understanding of how CO_2 and humidity affect the Li-air cell chemistry, since this is crucial for a device development (GIRISHKUMAR et al., 2010; WEN; SHEN; LU, 2015). In this context, one of the biggest issues regarding the carbon-based air electrode exposition to the ambient conditions is that it may lead to the formation of other compounds like Li_2CO_3 and LiOH instead of Li_2O_2 (MIZUNO et al., 2010; XIAO et al., 2011).

In addition to understanding products formation under ambient air, the Li-air cell demands concern from experimentalists working with device construction in order to find a device architecture wherein the distribution of Li^+ and O_2 enables a higher performance. Also, the question of how heterogeneous the triple-phase can be considered in terms of reactions mechanisms and, consequently, product formation has not yet been addressed.

Most conventional analytical techniques that has been used for Li-O_2/Li-Air batteries characterization offers limited descriptions of the reaction mechanisms, providing sensitivity that does not allow for resolving features smaller than a few micrometers. This is a barrier when studying the structure and chemical composition of sub-micrometer specimens used in batteries (LUCAS et al., 2015).

In view of that, synchrotron infrared nanospectroscopy (SINS) is a technique able to access opto-chemical properties of materials in the nanoscale, returning an infrared image together with topography, thus, fulfilling the lack of detail provided by conventional FTIR (HUTH et al., 2012). By performing SINS characterization during typical cycling cells (*operando*), we intended to investigate modifications on the surface along with changes of chemical composition of the system, aiming an understanding of the processes that take place on the electrode surface, especially regarding electro catalysis and electrolyte degradation. This investigation was complemented with a micro-

FTIR study, which explores large sample areas, producing a global view of the reaction and adding important information about this process.

All FTIR bands for each discharge product identified in this study is stated in Table 3.

Table 3: FTIR bands for Li-Air battery discharge products

Compound	Micro FTIR bands (cm^{-1})	SINS bands (cm^{-1})	Assignment
Li_2O_2	863	865	ν Li-O
Li_2CO_3	863	865	C=O
	1434-1474	1453	νCO
	1505	1501	νCO
LiOH	952	952	τ H2O
	1030	1018	ω, τ H_2O
DMSO	903	900	δCH
	1030	1018	νSO
	1337	1330	$\delta_s CH_3$
	1364 - 1402	1366 - 1406	$\delta_{as} CH_3$
$DMSO_2$	1290-1317	1298	$\nu_{as} SO_2$
$LiHCO_2$	1537-1568	1533-1565	δ_{as}COO

4.2 Methods

4.2.1 Cell design, electrode preparation and electrochemical operation

Li-O_2 traditional cells are a semi open system, closed at the anode side and open at the porous gas diffusion electrode side. However, the SINS technique only allows a study surface with a rugosity lower than 30 nm, which required adaptations on the cell design to make the porous cathode polished enough and opened in a way that it can be exposed to the AFM tip. The new design (presented in Figure 8) was manufactured by additive manufacturing, also known as 3D printing, using 316 Stainless Steel as substrate. The cell consisted of a base and a lid, separated by a Polytetrafluoroethylene (PTFE) insulating ring. The lid was subjected to grinding and polishing, from 80-100 mm coarse grinding to 1 µm diamond fine polishing, until it reached a rugosity as low as necessary (<30 nm). Is was then perforated to allow electrolyte access to the active material and subjected to Au sputtering process, since gold sputtered thin-films enhances the electric field of IR radiation due the surface plasmon polarization effect. The assembled cell and a scheme of cell design are presented on Figure 8 a and b, respectively. Figure 8c shows an illustration and a SEM image of the active material deposited on the working electrode.

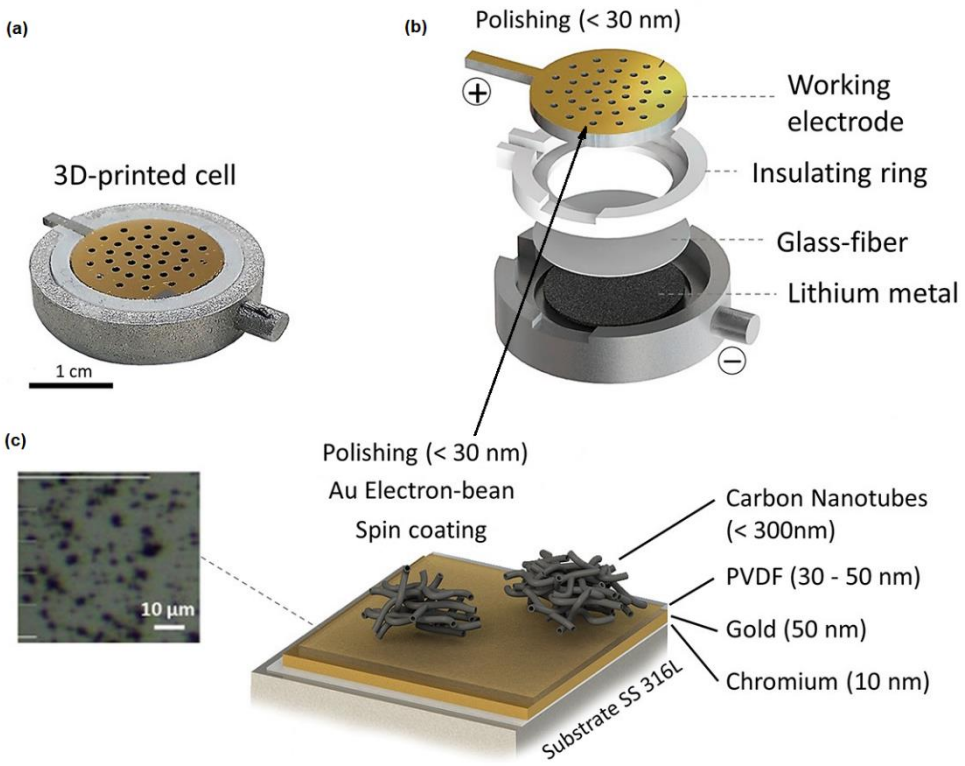

Figure 8: a) assembled cell; b) cell schematic design; c) gas diffusion electrode.

The air electrode was made by a catalyst layer deposited on the lid's surface by dropping an amount of a catalyst ink and using the spin coating technique to obtain a uniform film (inset Figure 8c). The catalyst ink consisted of a suspension of the active materials: carbon nanotubes (CNTs) (12,5 mg) and Nafion (50 µL), in a 5 mL isopropanol/water (3:2) mixture. The suspension was sonicated until it reached a homogeneous aspect.

Due to the system sensitivity to water, oxygen and other contaminants the cell was assembled inside an Argon filled glove box. A metallic Lithium foil, the anode, was placed on the base of the cell and topped with a Whatman glass fiber separator. A polymeric ring was then placed to isolate the two electrodes, followed by 137 µL of the electrolyte solution (0.1 M $LiClO_4$ in DMSO). Finally, the lid coated with the catalyst ink, that consisted of the cathode of the cell, was fitted into the ring (Figure 8b).

The assembled cell was stored inside an isolated chamber, removed from the glove box and transported to the IR1 beamline where it was immediately positioned on the sample holder and connected to the potentiostat for *operando* testing and characterization. The environment was purged with O_2 and kept with humidity levels below 6% during all the experiments.

The galvanostatic discharges tests were performed for characterization analysis using the micro-FTIR and the SINS techniques. The tests were conducted in a two-electrode configuration using metallic lithium as the reference and the counter electrode. An Autolab potentiostat/galvanostat (N series) was used to apply 100uA and 2uA for micro-FTIR and SINS characterization, respectively.

4.2.2 Synchrotron infrared nanospectroscopy (SINS) experiments

SINS experiments were performed at IR1 beamline at LNLS. In this station synchrotron radiation with THz to visible range frequency is collimated and coupled into a s-SNOM microscope (Neaspec GmbH). The IR synchrontron broadband beam is focused onto the metallic AFM tip (NCPt-Arrow or PtSi-NCH, NanoWorld AG). The tip acts as an antenna, which enhances the incident electrical field, producing a near-field light source with dimensions close to the size of the tip apex (~25 nm radius). The sample is placed close to the tip (70-90 nm), which provides a local polarization of the sample.

The tip-sample scattering is detected in a mercury cadmium telluride detector (MCT, KLD-0.1, Kolmar Technologies Inc.).

The measurements were performed in a range of 700 to 1800 cm^{-1}, with a spectral resolution of 20 cm^{-1}. Points were analyzed on an area of 150 x 150 pixels with a 20,1 ms integration time. A pure gold surface was used as reference and all samples results were already normalized. *In situ* measurements of the cathode were performed immediately after cell discharge. Points spectrum were obtained due the high heterogeneity of the cathode surface. The Nano-FTIR spectra was collected in triplicate and the presented results are an average of each region (see Figure 11). This procedure was important to enhance the FTIR signal compared with the noise. Data acquisition from the charged battery was not possible due the charge influences in the electrical field of the AFM tip.

4.2.3 Micro-FTIR experiments

The micro-FTIR measurements were carried out in a FTIR spectrometer (Cary 600, Agilent Technologies) with a mercury cadmium telluride detector. A microscope (Cary 600, Agilent Technologies) is coupled to the FTIR spectrometer, which allows the analysis of micrometric regions of the sample. The spectra were collected in the mid-infrared range (4000-800 cm^{-1}), with 8 cm^{-1} spectral resolution and 100 scans, using a x25 objective. Infrared reflection mode was used for data acquisition due to the non-transparency of the samples. In the battery, the gold nanolayer of the cathode tends act as a surface enhanced infrared spectroscopy. *Operando* micro-FTIR measurements were collected during the discharge process. Thanks to the microscope, images of the cathode surface were captured during cell operation. All the spectra were normalized by gold reference.

All the IR experiments of this research used resources of the Brazilian Synchrotron Light Laboratory (LNLS), an open national facility operated by the Brazilian Centre for Research in Energy and Materials (CNPEM) for the Brazilian Ministry for Science, Technology, Innovations and Communications (MCTIC). The IR1 beamline staff is acknowledged for the assistance during the experiments.

4.3 Results and discussion

Figure 9 presents the discharge profile obtained before the FTIR analysis by micro-FTIR and SINS using 10 µA and 2 µA current, respectively. Lower potential was reached during the discharge profile for micro-FTIR due to the higher current density (500mA g^{-1}) (CHRISTENSEN et al., 2011). The lower potential shown in Figure 9 a is in the range of the solvent electrochemical stability window (0,1 to 4,7V) and thus the discharge potential used does not affect the DMSO stability (AURBACH, D., 1999; MOZHZHUKHINA; MÉNDEZ DE LEO; CALVO, 2013).

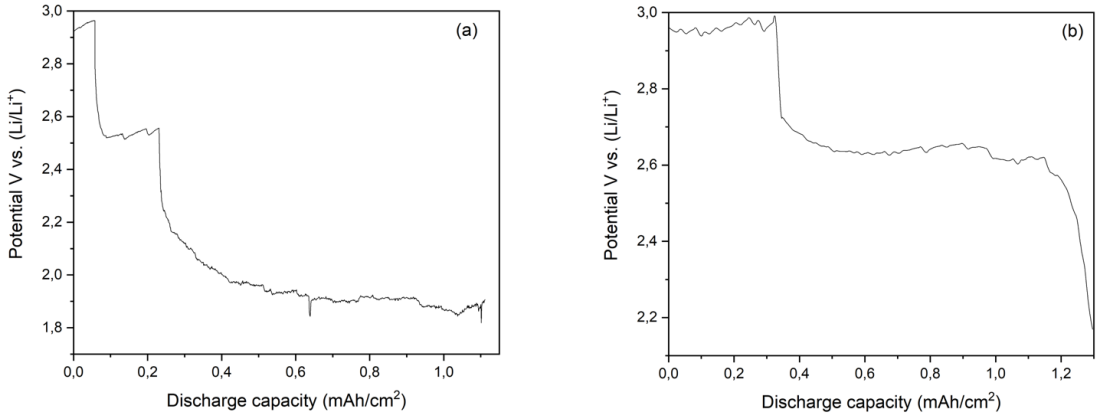

Figure 9: Discharge profile obtained for a) micro-FTIR and for b) SINS characterization

The measurement using SINS spectra was performed after a 1.28 µAh cm^{-2} discharge analyzing two different regions with a 25 nm space resolution. For an improved signal-to-noise ratio, each presented SINS spectra represents an average of three SINS point spectra acquired on the same location. This procedure was important to enhance the FTIR signal compared to the noise. Figure 10 presents the average nano-FTIR spectra, obtained from subsequent Fourier transform of the corresponding interferograms, for both 1 and 2 regions.

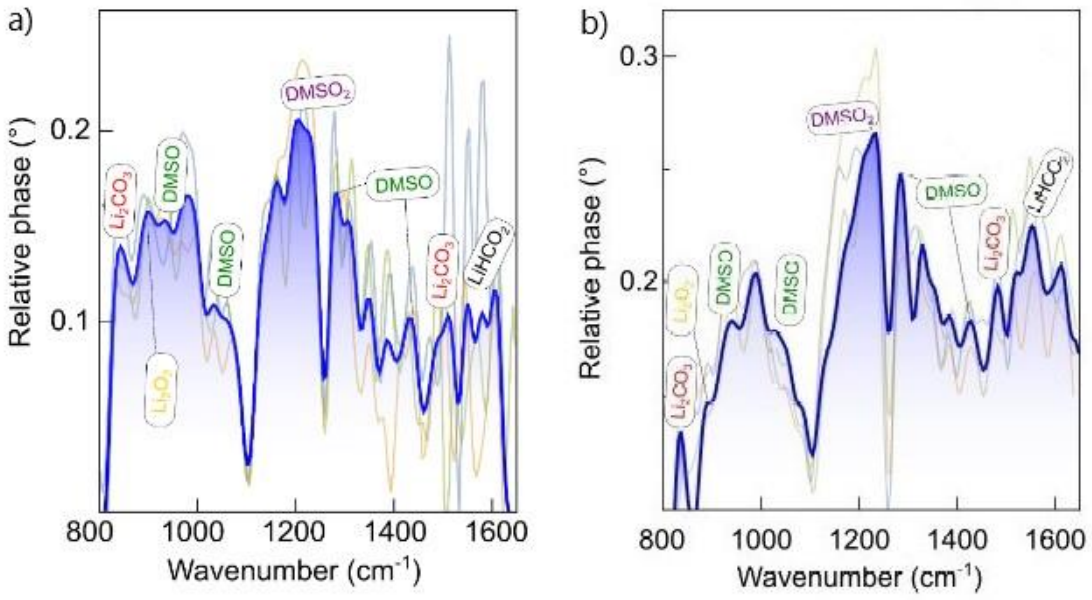

Figure 10: SINS phase spectra from Regions a) 1 and b) 2.

The AFM image of the cathode area analyzed with the FTIR technique is presented on Figure 11 a. 3D image of the topography after the discharge process reveals the irregular morphology of the air electrode (Figure 11 b). Typical Li-Air cathodes are porous, with a wide pore size distribution and irregular features. It was important and necessary that the *in situ* cell electrode represented well the real system, but respecting the technique limitations. Touching these two points together comprised a significant challenge, since they are opposite characteristics. In both images (Fig. 11 a and b), dark regions are observed indicating the presence of carbon, a strong light-absorbing material.

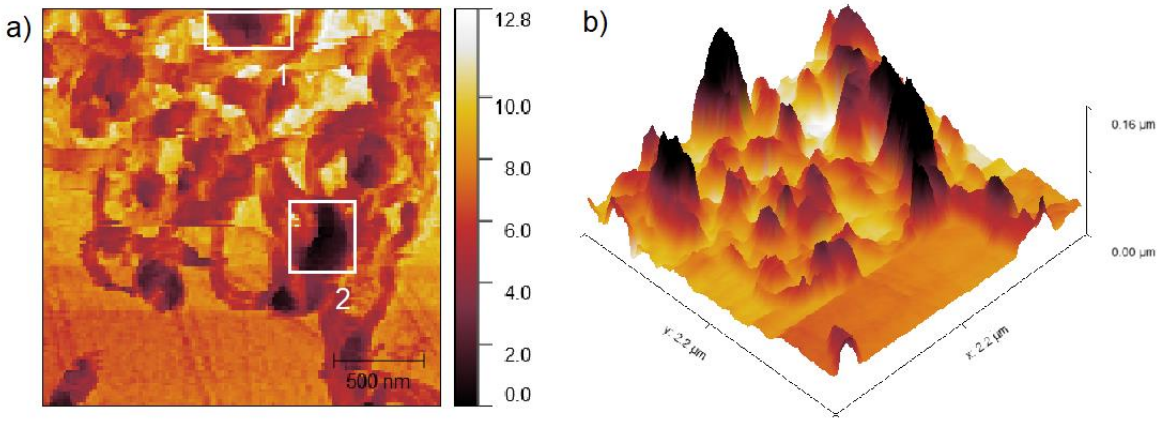

Figure 11: a) AFM image of the cathode electrode; b) cathode 3-D topography during SINS

For the micro-FTIR technique the result was obtained after a 1.11 µAh cm^{-2} discharge with a 20-micron space resolution. The FTIR obtained with micro-FTIR technique is presented in Figure 12.

For both analyses, the spectra region was selected aiming a three-phase zone, which refers to carbon nanotubes, electrolyte and gas phase. Considering a qualitative analysis, we suggest a surprisingly homogeneous product formation over the carbon nanotubes, since all the formed species were both present at the two nano-meter size spots and as the average from the micro-FTIR analysis and no distinction could be made at this level. The same characteristic bands related to the different products of Li-air battery were clearly observed. All the bands from the SINS spectra and micro-FTIR can also be seen with more precision in Table 3, in which all the bands for each identified discharge product is thoroughly demonstrated.

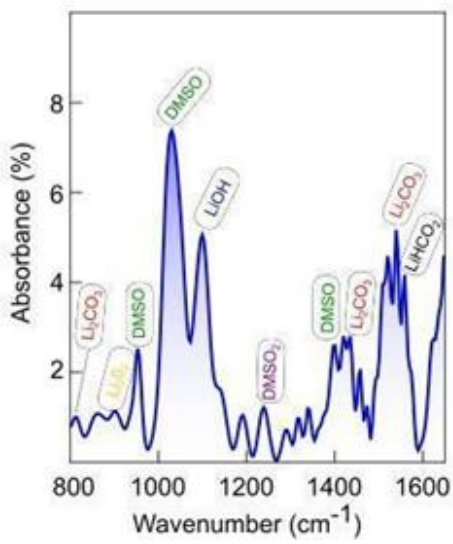

Figure 12: micro-FTIR spectrum

It is possible to verify bands in wavenumber range characteristic of the discharge products for Li-air batteries, namely: lithium peroxide (Li_2O_2), lithium carbonate (Li_2CO_3), lithium formate ($LiHCO_2$) and lithium hydroxide (LiOH). Moreover, the dimethyl sulfoxide (DMSO), solvent used in the electrolyte, and its main decomposition product, dimethyl sulfone ($DMSO_2$). The results also indicated that the discharge product's chemical composition is not related with the discharge rate, since the micro-FTIR experiment was conducted applying a discharge current 5 times higher. Using pure O_2 and a current range 100 times higher, Read reported that increasing

discharge rate the oxygen concentration in the electrolyte was reduced, leading to Li_2O formation preferentially, instead of the Li_2O_2 (READ, 2002). Thus, our results reveal that in the presence of humidity and CO_2, with different parallel reactions, a significant increase in μA scale is not enough to influence the chemical products composition.

The only difference is that the relative intensities of the peaks of the micro-FTIR spectrum differ from those in the SINS spectrum. This stems from the fact in SINS the optical near field is predominantly polarized along the tip axis (MULLER et al., 2016). Hence, the modes with the infrared dipole moment parallel to the tip axis present higher amplitudes than those with the infrared dipole moment perpendicular to the tip axis. Consequently, the relative intensities of the peaks in the SINS spectrum is dictated by the molecular ordering in the probed nanodomain, which can randomly vary in our system that does not have a uniform preferential order. In the micro-FTIR spectrum, the excitation is not polarized and the relative peak intensities are related to the average concentration of the molecular species in the illuminated area. These results reveal the potential of the SINS spectra technique on the Li-Air technology ripening process, investigating local reaction mechanisms that could also be used to address the role of dispersed electrocatalysts on carbon matrices.

Following the micro-nano comparison, we have also investigated the dynamics of the previously tested electrodes over their discharge products composition, searching for further information regarding Li-air batteries during operando experiments in micro-FTIR. Measurements started with the OCP (open circuit potential) operation regime up to 2300 s of discharge using a 100 μA current (Figure 13).

Regarding the discharge profile, the potential decreased fast, achieving 2.0 V in 2300 s, which was expected by the high current applied during the discharge procedure, considering the substantially low mass of active material in the cathode (μg range). This current was used to enhance the discharge products formation, however decreased battery lifetime.

Here we also considered the spectra from a three-phase zone, ensuring an area with a higher probability for the discharge products to be formed and detected (Figure 11a). Moreover, we did not observe discharge products in a cathode surface with CNT and without electrolyte as shown in Figure 14 emphasizing the need of three phase zone.

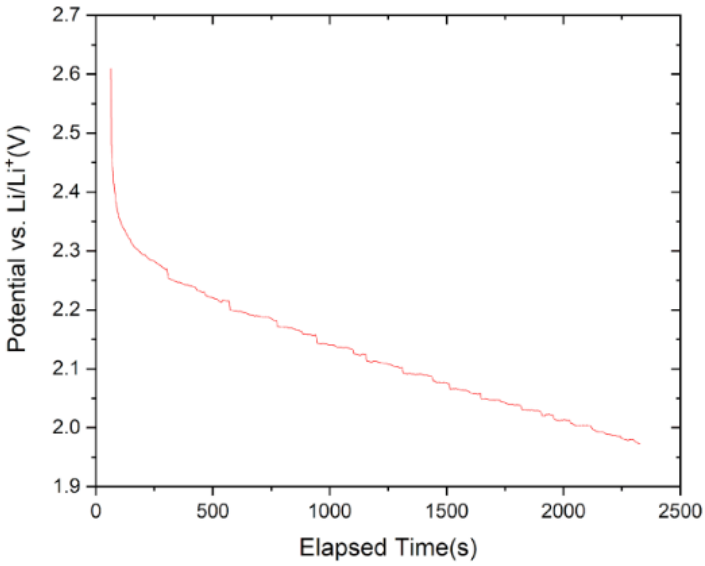

Figure 13: Discharge profile obtained by operando micro-FTIR characterization

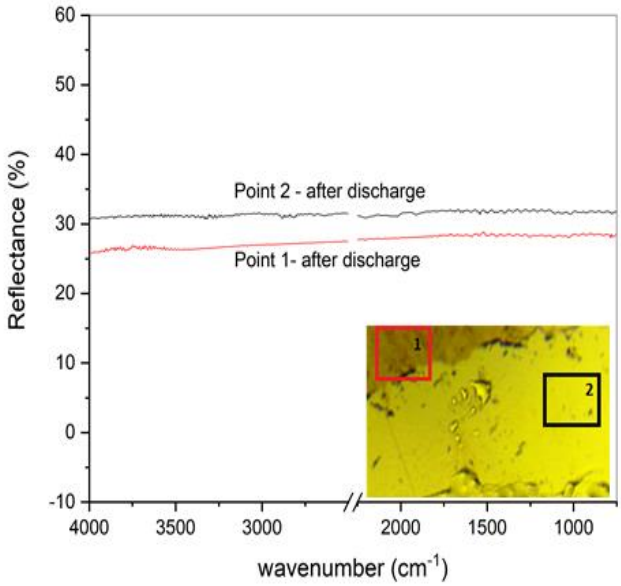

Figure 14: micro-FTIR spectra of cathode surface with only CNT over gold after galvanostatic discharge.

The *operando* micrographs and spectra obtained from micro-FTIR are presented in Figure 15. The micrographs (Figure 15 b) show dramatic changes on the cathode surface as a function of the discharge temporal evolution. This indicates a possible agglomeration of reaction products. We can also point out more pronounced changes near the CNT surface but also near the gold/CNT substrate, indicating the nucleation on both for the discharge reactions. Au and CNT are known as good materials

for air cathode in Li-O_2 batteries and the catalytic effect of Au-supported nanoparticles has been proved (GITTLESON; RYU; TAYLOR, 2014; GITTLESON et al., 2015; WANG et al., 2015; SUN et al., 2017). However, our substrate is a flat Au surface mainly for FTIR signal enhancement, therefore we do not expect any major action over the discharge.

Initially we analyzed the air electrode with the electrolyte salt (0.1 M $LiClO_4$ DMSO) (Figure 15 c). The DMSO bands are presented at ~ 1435 and 1406 (δasCH3), 1315 (δsCH3), 1030 (νSO) and 950 cm^{-1} (δCH). Bands characteristic of $LiClO_4$ were not verified, likely due to the low molar ratio of the salt, 0.007:1 (WANG et al., 1997; SCHROEDER et al., 2015; VIVEK et al., 2017). For the air cathode and following the Li-air battery discharge elapsed time, the spectra shows the DMSO presence and increasing intensities of the following bands characteristic of discharge products at 140 s: 3750, 1800, 1745, 1650, 1620 1505, 1455, 1435, 1200, 1080, 1030 and 940 cm^{-1} (Figure 15 c). These bands confirm the maintenance of the reaction route during the discharge process.

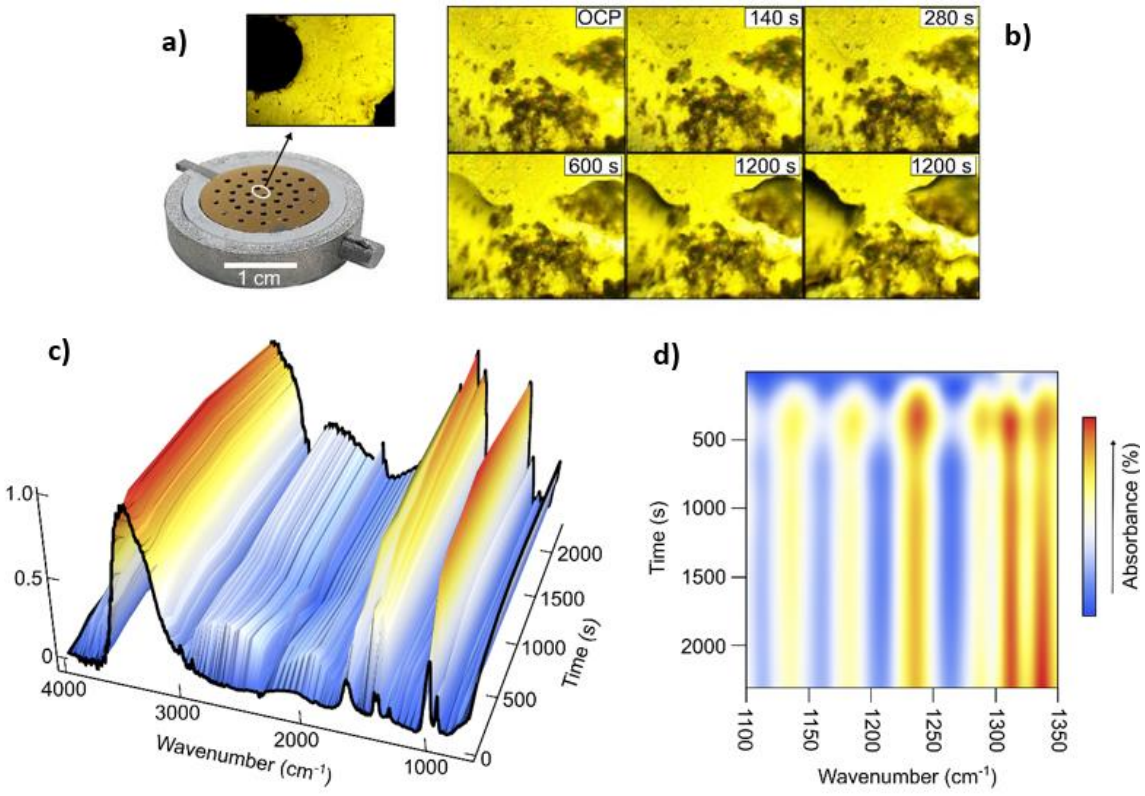

Figure 15: a) Analyzed area with 5 times amplification; b) Micrographs with 25 times amplification; c and d) Infrared spectra with elapsed time of cell discharge.

FTIR spectra of the discharge process (Figure 15 d) reveals the permanence of the DMSO band and the appearance of the bands at 1142 and 1184 cm^{-1} which correspond to the symmetric stretch of the SO_2 group (νsSO_2) in dimethyl sulfone ($DMSO_2$) combined with the increase of bands due to the asymmetric stretch of SO_2 ($\nu asSO_2^-$ 1230, 1293 and 1335 cm^{-1}). Those new bands are assigned to DMSO degradation products (AURBACH et al., 2009; MOZHZHUKHINA; MÉNDEZ DE LEO; CALVO, 2013; SHARON et al., 2013). The dimethyl sulfone ($C_2H_6O_2S$) can be formed by the DMSO reaction with the lithium discharge products and/or with the superoxide anion (O_2^-) (Equation 14) (MOZHZHUKHINA; MÉNDEZ DE LEO; CALVO, 2013). This DMSO decomposition was reported using KO_2 and during the storage of electrodes after discharge experiments due to the reaction with Li_2O_2 (Equation 15 and 16) (MOZHZHUKHINA; MÉNDEZ DE LEO; CALVO, 2013; KWABI et al., 2014; SCHROEDER et al., 2015). In the present work we report a fast DMSO degradation under discharge operando measurement, which had not been observed yet. We also suggest that in our system, the decomposition of the electrolyte occurs ($DMSO_2$) due to the reaction with Li_2O_2 since it was reported 1.3 V as the electrochemical potential difference between O_2- and O_2^{2-} in DMSO.

$$2O_2^- + 2C_2H_6OS \rightarrow 2C_2H_6O_2S + O_2^{2-} \quad (14)$$

$$C_2H_6OS + Li_2O_2 \rightarrow C_2H_5OLi + LiOOH \quad (15)$$

$$LiOOH + C_2H_6OS \rightarrow C_2H_6O_2S + LiOH \quad (16)$$

The micro-FTIR (Figure 15 c) spectra show bands located at 1780, 1200, 1080 and 870 cm^{-1} which are typical of lithium peroxide (Li_2O_2) (FREUNBERGER et al., 2011a). Considering the discharge reaction, we explain the formation of Li_2O_2 by the disproportion reaction (Equation 19), that follows the oxygen reduction (Equation 17) and the ions Li^+ complexation (Equation 18), which are necessary to produce O_2^- and LiO_2 (solid solution-based superoxide) before it.

$$O_2 + e^- \rightarrow O_2^- \quad (17)$$

$$O_2^- + Li^+ \rightarrow LiO_2 \quad (18)$$

$$2LiO_2 \rightarrow Li_2O_2 + O_2 \quad (19)$$

For aprotic Li-air batteries the formation of Li_2O_2 is ideally expected. However, in this case, different products are anticipated due to atmospheric (Air)

conditions. When H_2O and CO_2 are present in the system, as in the experiments described here, it was suggested that Li_2CO_3 and lithium hydroxide species form even in aprotic solvents (CARVALHO et al., 2019). We experimentally show the presence of Li_2CO_3 identified by its characteristic bands at 1500, 1450, 1080 and 870 cm^{-1} (MIZUNO et al., 2010). The intense bands centered at 1450 and 1500 are attributed to the νCO (NIST) vibrational mode. The 1080 and 870 cm^{-1} bands are assigned to Li_2O_2 and Li_2CO_3, respectively. Our interpretation is that a spontaneous chemical degradation of Li_2O_2 into carbonate when in contact with CO_2 occurred (GOWDA et al., 2013). It is well known that Li_2CO_3 is more thermodynamically stable than Li_2O_2 and the Li_2O_2 formed could react with the residual CO_2 contained in the ambient atmosphere to form Li_2CO_3 (Equation 20), as following:

$$Li_2O_2 + CO_2 \rightarrow Li_2CO_3 + ½\ O_2 \qquad (20)$$

4.4 Conclusion

We assessed the infrared vibrational signature of lithium-air batteries in the micro and nanoscale using micro-FTIR and SINS spectroscopies. First, we introduce a new cell design, with a carbon-based cathode adapted for the open cell. Using the same cell for *in situ* testing, both techniques provided valuable information about the formation of discharge products and electrolyte degradation. The results emphasize the importance of triple-phase for the discharge reactions to happen and that even with cathode surface heterogeneity the detected discharge products were the same using the micro and nano scale analysis despite the difference on the discharge rate. By micro-FTIR characterization the system was also studied under *operando* operation, which suggested DMSO degradation due to the interaction with Li_2O_2, forming $DMSO_2$. Based on these findings we highlight the applicability of multi-scale FTIR techniques and emphasize it as an important tool to study complex discharge processes typically found in conversion batteries as the case studied here for lithium-air.

CHAPTER 5

Redox Mediators' exploratory studies and the operando synchrotron XRD investigation of LiI as redox mediator in Li-O_2 batteries

5. Redox mediators' exploratory studies and the *operando* synchrotron characterization of LiI as redox mediator in Li-O_2 batteries

5.1 Introduction

The research proposal for this doctoral thesis started with developing *in situ* and *operando* characterization of typical Li-O_2 cells. Afterwards, motivated mostly by the fact that there was barely published paper demonstrating time-resolved redox mediated Li-O_2 batteries characterization, we faced a growing interest in studying the effect of the redox mediators' addition in the system. The studies reported from this point on include the use of redox mediators in the Li-O_2 system.

In the Literature Review chapter, there is a brief introduction to the tree classes of compounds that comprise the Redox Mediators. In this chapter, we present the preliminary results of the performance of an organometallic (heme) and two halides (LiI and LiBr) as RMs and a more detailed investigation regarding the use of LiI.

The halides were selected for this study due to the fact that this is the class of compound that, based on literature, presents the least drawbacks. The organometallic one, heme, was selected for the lack of papers published describing its performance in Li-O_2 batteries. Heme is a biomolecule, an iron protoporphyrin, component of hemoglobin, that binds directly with oxygen (PARK et al., 2018).

In the presence of RMs, charge reactions usually occur according to the reactions in Equations 10 to 12 (section 2.5), which is why the charging potential of the Li–O_2 cell is around the redox potential of the RM (PARK et al., 2018). The electrochemical behaviour of the system depends on all of its components, the electrolyte's solvent and ions, concentration, the environment of the test (BARD; FAULKNER, 2000). For being so particular, the behaviour of each system will be studied and presented here, this investigation allows a deeper understanding of how the RMs acts on the Li-O_2 system electrochemically.

5.2 Methods

5.2.1 Gas diffusion electrodes synthesis

Multi-walled carbon nanotubes (MWCNT) grown on a stainless-steel mesh were used as gas diffusion electrodes. The substrates (AISI 304L M100 0.1 mm mesh wire diameter and 0.15 mm × 0.15 mm mesh pore size) were cut off in 2 cm diameter discs and then they went through ultrasonic cleaning in isopropanol. After dried, the discs were placed on a tray and wetted with a nickel nitrate alcohol solution (3.6 g in 125 mL ethanol), which acts as a catalyst for the growth process. The set was inserted into the furnace where the CNTs growth was performed by the floating catalyst based chemical vapor deposition method (FC-CVD). The furnace was purged with 1000 sccm of N_2 for 10 min to mitigate oxygen content from inside. With the inert N_2 atmosphere, furnace temperature was increased at a rate of 65°C min^{-1} up to 750 ºC and maintained throughout the MWCNTs growth process. In order to grow MWCNTs onto the AISI mesh, 15000 sccm of 43.6 wt% Camphor ($C_{10}H_{16}O$) and 2 wt% $Ni(NO_3)_2$ ethanol solution (C_2H_5OH) were carried into the FC-CVD by N_2 gas for 15 min. At the end of the growth process, electrodes were weighted on a microbalance (XSE205DU, Mettler Toledo Switzerland), the ones with masses on the range 2.5 ± 0.3 mg were selected for testing.

5.2.2 Cell assembly and battery cycling

Due to lithium sensitivity, cell assembly took place in an Argon atmosphere glove box (MBRAUN-LABstar Workstation), avoiding contact with water, oxygen and nitrogen. A metallic lithium disc (Tob Machine, 99.99%) was used as the cell's anode, dimethyl sulfoxide (DMSO) (Sigma Aldrich, 99.99% anhydrous) was the solvent used for electrolyte preparation. Electrolyte solutions consisted of 0.1 M $LiClO_4$ (Sigma Aldrich, 99.999% anhydrous) + RM in DMSO (Sigma Aldrich, 99.99%). The RM concentrations were: 50 mM LiBr, 50 mM LiI and 2 mM heme. All the described materials were exposed only to Argon atmosphere.

Cycling tests were performed on a homemade Swagelok type cell (Figure 16) machined for the experiments. It has been used by the research group in the past years. The cell was sealed between two stainless steel plates containing oxygen inlet/outlet terminals. The plates were isolated by a Teflon chamber and the current collectors were

located on the plates which during cell testing were connected to a potentiostat/galvanostat for data acquisition.

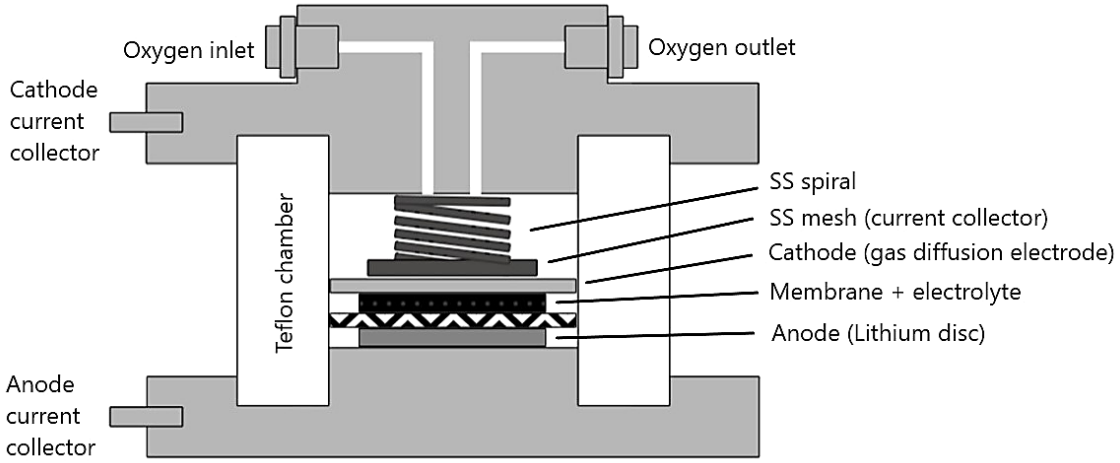

Figure 16: Scheme of the electrochemical cell used for battery cycling.
Source: FRANCISCO, 2020.

For assembly, the metallic disc foil was placed on the counter electrode plate, subsequently, the 100 µL of the electrolyte solution was added over a Whatman Millipore glass fiber separator placed on the top of anode, followed by the prepared gas diffusion electrode. Cells were properly sealed and let rest assembled for 72 h before removed from the glove box and tested externally.

Before cycling, the cells were purged with O_2 for 10 minutes at a flow rate of 0.3 $L.min^{-1}$ in OCP. Tests were carried out galvanostatically with a 33.3 mAg^{-1} current density on a potential window from 2.4 to 4.0 V. The cycles were capacity limited. After cycling, cells were purged with N_2 and opened inside the glovebox to prevent electrode contact with the air and contamination. Samples were kept in the inert environment until subjected to further characterization when the *ex situ* characterization was applied.

5.2.3 Synchrotron XRD characterization

This part of the research used resources of the Brazilian Synchrotron Light Laboratory (LNLS), an open national facility operated by the Brazilian Centre for Research in Energy and Materials (CNPEM) for the Brazilian Ministry for Science, Technology, Innovations and Communications (MCTIC). The XPD beamline staff is

acknowledged for the assistance during the synchrotron XRD characterization experiments.

The XPD beamline operates on the range of 5-15 keV and has 4+2 circles diffractometer. This diffractometer allows the installation of reaction cells, furnaces and cryostats. A strip detector Mythen 1K was installed at 1m from de diffractometer for fast acquisition of X-ray diffraction patterns. In this configuration, the angular resolution is 0.03º (FWHM) and the detector acquires 3.5º at one time in the 2-theta range. The studies were carried at 7 keV (λ = 1.771 Å) energy and the cycling conditions were the same described for the electrochemical studies.

El Cell® Opto Std cell topped an adapted lid with a Mylar® window (X-rays transparent) was used as sample holder, since it had been previously tested and identified as a successful closed cell, avoiding electrode contamination.

5.2.3.1. *Operando* synchrotron XRD characterization

Cells used for the *operando* tests were built in an El Cell® Opto Std cell with a stainless-steel lid specially developed by our research group using 3D printing with stainless-steel for the tests. The designed lid has a gas chamber topped with a Mylar® window, which is transparent to X-rays. Figure 17 shows the image of the cell assembling scheme (a) and coupled with the lid (b).

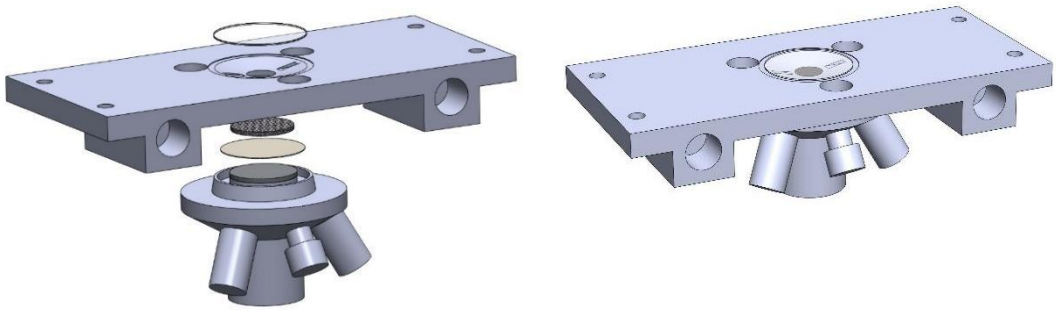

Figure 17: *Operando* XRD cell a) assembling scheme; b) coupled with the lid

5.2.4. SEM characterization

The surface morphology of the scaffold was examined using a FEI high speed Inspect F50 scanning electron microscope at the Brazilian Nanotechnology National Laboratory (LNNano).

5.3 Results and discussion

5.3.1. Redox mediators' exploratory studies

Primary investigation on the effect of redox mediators in Li-O_2 battery was performed. Capacity limited cycling, using the MWCNT electrodes described in the Methods sections, were conducted. First, we compared the cycling profile of two first cycles, limited to 500 mAh/g_c, with and without LiI (Figure 18 a and b, respectively).

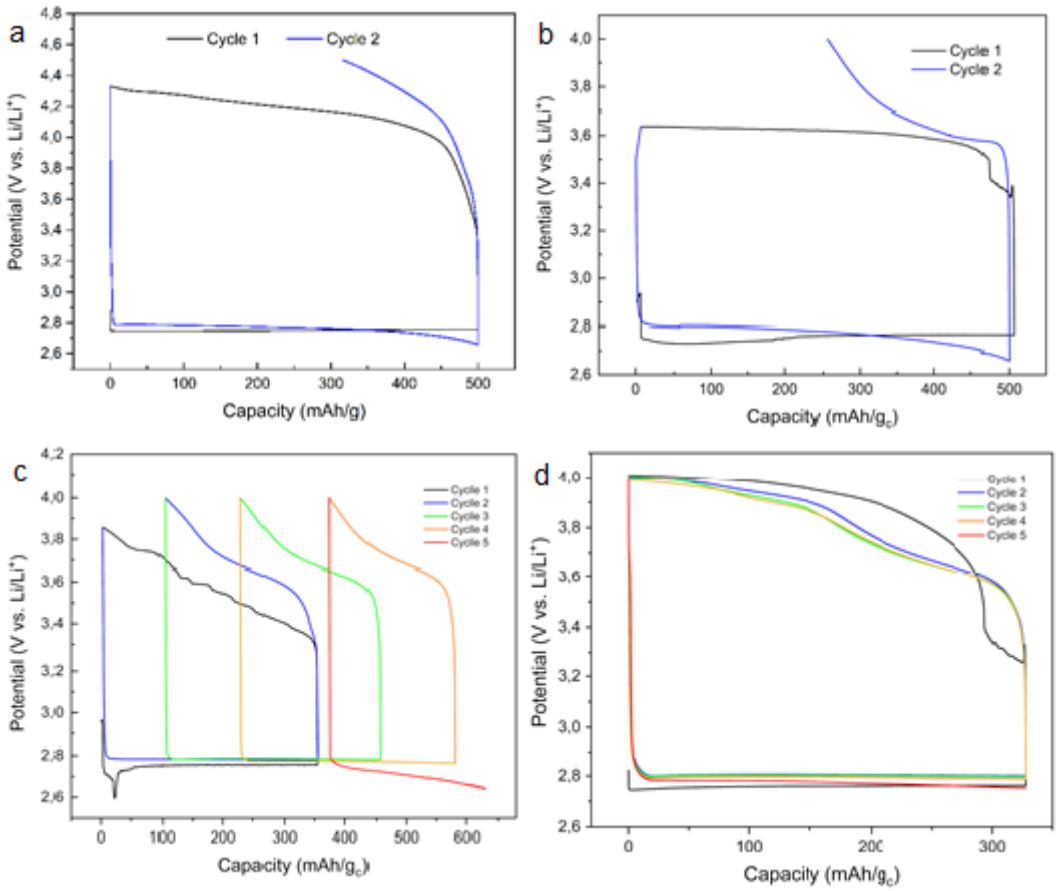

Figure 18: Cycling profiles with capacities limited to a) 500 mAh/g_c without any RM; b) 500 mAh/g_c with LiI; c) 350 mAh/g_c with; heme; d) 333 mAh/g_c with LiBr

The potential window limited for the system without any mediator was set up to 4.5 V. Previous tests indicated that this system would reach 4 V rapidly, and for comparison reasons a higher cut-off was settled. Regarding discharge we can observe that the two plateaus for both systems were practically the same, with no significant differences. For charge, on the other hand, there was a substantial decrease in the plateau when LiI is used, with a 0.6 V lower charge overpotential. Since higher overpotentials mean higher energy loss, a decrease like that is an important improvement to the system energy efficiency. Besides that, this reduction also allows the cell to operate in a narrower potential window, reducing the formation of by-products due to decomposition of the cell's components, such as electrolyte.

These results are consistent with others found in literature, where LiI addition to the system showed, in some cases, even greater overpotential reductions (LIM et al., 2014; QIAO et al., 2017). The second charge with LiI was interrupted before it reached a plateau because we choose to study the mediated systems in a window limited to 4 V, since this overpotential reduction was exactly the aim with the RMs addition.

Figures 18 c and d shows the cycling profiles of the systems with addition of heme and LiBr as redox mediators, respectively. These two mediators also decreased the charge overpotential, and despite the fact that this reduction was smoother than with LiI, more cycles were achieved in the determined potential window. The cell with heme did not reach a plateau even with a capacity 1.5 times lower compared with LiBr.

The electrodes from the cycling shown in Figures 18 b, c and d were subjected to XRD ex situ characterization. The XRD patterns are presented in Figure 19.

The diffraction peaks at $2\theta = 37.5^{o}$ and 41.3^{o} are assigned, respectively, to (101) and (110) planes, of lithium hydroxide tetragonal symmetry (LiOH JCPDS No. 32-564). The others, with $2\theta = 38^{o}$ and 40.4^{o}correspond to lithium peroxide (Li_2O_2 - JCPDS No. 09-0355) (100) and (101) planes of hexagonal structure.

Despite the difference in the number of cycles each system underwent before the electrodes were characterized, in the systems mediated by LiI and LiBr we can only see formation of LiOH. In the XRD pattern of the bromide mediated electrode, we can suspect of a discreet (100) Li_2O_2 peak, but it is hard to confirm with the (101) plane since it is located close to the broad diffraction peak at $\approx 40.7^{o}$, which is related to the electrode substrate.

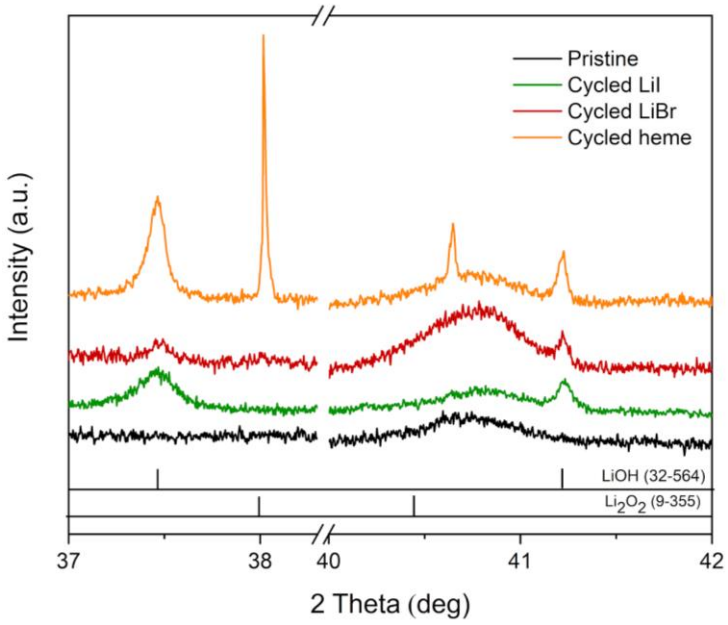

Figure 19: XRD patterns of the electrodes after cycled with RMs

Kwak and co-workers (2016) compared the products formed in a Li-O_2 cell in the presence of LiI and LiBr, with some water content. They observed the formation of LiOH in the iodide mediated system, while with LiBr the discharged cathode exhibited peaks characteristic of crystalline Li_2O_2 only. This result differs from the one we show here. The formation of different products in each of these two mediated systems is discussed in more depth in the following section for LiI and in Chapter 6 for LiBr, respectively.

Concerning the products composition revealed by the electrode of the heme mediated cycling, we observe clearly the presence of LiOH and Li_2O_2. The location of Li_2O_2 (101) plane peak is slightly dislocated due to the interaction with the substrate peak, but the intensities and locations of the others leave no doubt of the presence of both products, which are even more crystalline. There aren't many studies using iron mediation in the Li-O_2 system. Sun et al (2014) investigates the use effect of iron phthalocyanine (FePc) as redox mediator in cells with DMSO and TEGDME-based electrolytes, always with LiTFSI. They observed Li-peroxide grows and decomposes without direct contact with carbon, promoting an enhanced electrochemical performance, especially with DMSO as solvent, which batteries were able to tolerate higher discharge and charge current densities. With heme, specifically, there is probably only one published paper reporting its use as RM, showing the chemical change of heme redox molecules in the

$LiClO_4$ + TEGDME-based cells (RYU et al., 2016). None of these studies observed the formation of LiOH, only Li_2O_2 and LiO_2 were described as discharge products.

In terms of charge profile, the fact that heme mediated cycling did not reach a charge plateau is consistent with the study previously mentioned, where the plateau was only observed above 4 V, which may be a disadvantage when compared to halides. And still, the solvent used in the electrolyte is different from the one we used here. Their results with heme indicated a strong synergistic effect between the porphyrin and the electrolyte used, specially the Li salt employed. Despite the fact that porphyrins and phthalocyanine are molecules with multiple similarities (GOTTFRIED, 2015), bonded in a similar manner (PRZYWARSKA-BONIECKA; TRYNDA; ANTONINI, 1975), and considering that the metal ion is the same in the molecules used, deeper investigation should be conducted for a more appropriate comparison between those two studies and this one.

5.3.2. *Operando* synchrotron XRD investigation of LiI as redox mediator in Li-O_2

Operando XRD characterization of the system with LiI as RM is shown in Figure 20, that shows the diffractograms of the electrode as the cell discharged progressively.

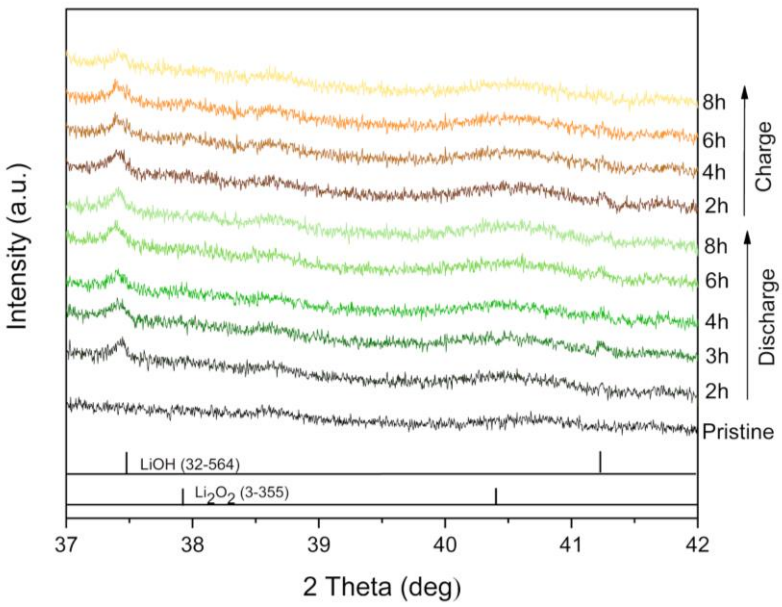

Figure 20: Operando XRD characterization of Li-O2 cell with LiI as redox mediator

The low intensities of the signal, comparing to other results obtained (Figure 24 a, 25 a and b), are more likely to be due to a local low concentration of compounds, since the total amount of active material on the electrode and the SS scaffold substrate are very similar in both analyzed systems. Qualitatively, we can see that the LiOH formation can be identified in the first XRD pattern, measured 2h after starting the discharge. There was a minor increase in the ~37.5º LiOH peak with time, while the ~41.2º peak showed a slight growth from 2 to 3h, maintaining roughly the same intensity until the end of the discharge step. Regarding the Li_2O_2 characteristic peaks, it can be barely identified, so we would say that only LiOH was formed in this process. During charge, we would expect the intensities of the peaks to decrease with time, however, only the 8-hour charge pattern show a small reduction from the previous pattern intensity. It means that the product decomposition was considerably slower than the formation, even with the LiI as mediator, which is expected to favour the Lithium oxides species decomposition (PARK et al., 2018).

After the discharge-charge process the cycled electrode was analyzed by SEM. Looking at Figure 21 a we can see how discharge products overload the electrode surface, completely clogging the voids. Zooming the image to twice that magnification (Figure 21 b), we can see the nanotubes surrounded by clusters of products. These images confirm the XRD result showing that despite the charge, that lasted almost the same time of the discharge, there was still a substantial amount of discharge products deposited on the electrode surface.

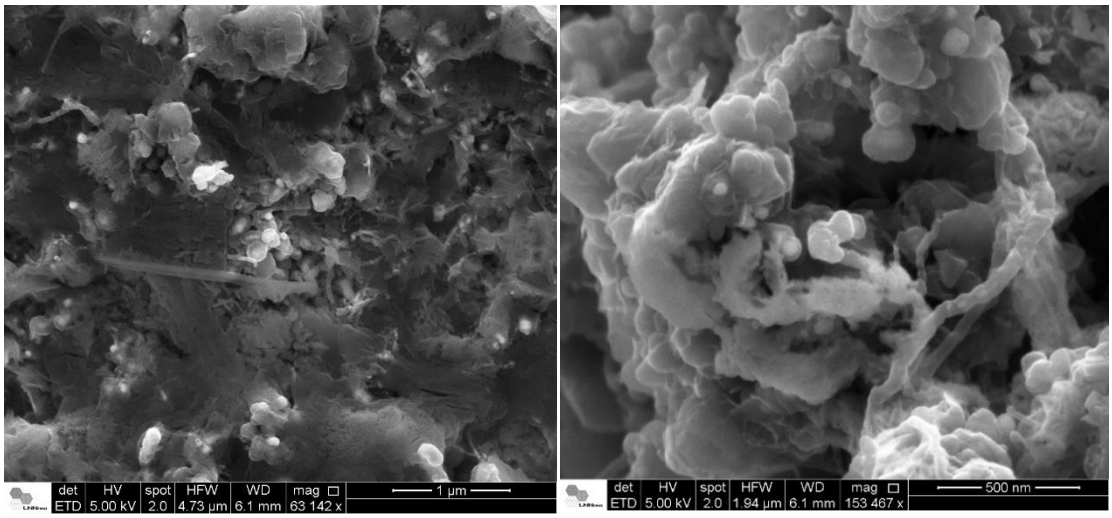

Figure 21: SEM images of the LiI mediated *operando* characterized electrode.

Comparing the XRD patterns of cells that underwent *operando* characterization with LiI and without any mediator, it is very clear that in the mediated cycle there was a difference on the discharge products detected (Figure 22).

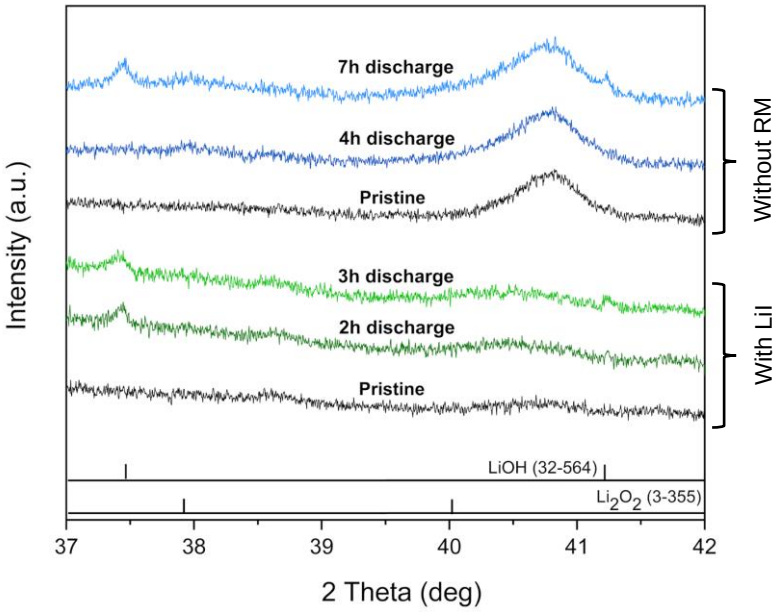

Figure 22: Time comparison for discharge products XRD detection, with and without RM

With the mediator only LiOH was formed. In the absence of LiI, previously to LiOH formation, Li_2O_2 can be identified in the XRD pattern. This qualitative analysis agrees with some results previously published in the following studies. Qiao and co-workers (2017) shows that LiI promotes nucleophilic attacks that catalyzes the decomposition of Li_2O_2, resulting in LiOH accumulation. Another study, comparing the Li-O_2 system in the absence and presence of LiI, reveals that in the last case, LiOH crystallites are formed by a particle- by-particle nucleation and growth process (LI et al., 2017). Burke *et al* (2016) suggest that an electrolyte containing LiI and water at impurity levels induces LiOH formation, which is not reversible with charge, thus leading to multiple side reactions. Zhu and coworkers (2017) conducted titrations of Li_2O_2 and LiOH with I_3^- in the presence of water and identified that LiOH oxidation reactivity is the lowest toward the oxidation by I_3^-. Those are all hypothesis that would explain why even after an 8-hour charge our *operando* XRD, there was barely no decrease in the intensities of the peaks related to LiOH. The cited studies, however, investigated DME-based systems.

There are not many studies using DMSO. Nakanishi and co-workers (2018) compared LiI-mediated systems with TEGDME and DMSO-based electrolytes through a combination of galvanostatic cycling, electrochemical mass spectrometry. In the DMSO-based system, the charge plateau around 3.3 V observed suggested that there was no formation of molecular iodine, so the mediation would be based on the reaction between I_3^- and Li_2O_2. The same was not observed in the TEGDME-based electrolyte, where two charge plateaus indicated the occurrence of both $3I^- \rightarrow I_3^- + 2e^-$ and $2I_3^- \rightarrow 3I_2 + 2e^-$ reactions. The authors concluded that mediation reactions were more stable in this DMSO system than the corresponding TEGDME system. Comparing that study with ours, their LiI concentration was twice the one used in this study, and the electrolyte salt concentration was 1 M, while here it was 0.1 M. Capacity-wise, both studies has cycles with capacity limited to 0.25 mAh cm^{-2} (here we choose to normalize the capacity per mass of active material, but converting for comparison we have a normalization per area close enough to the one described in the study).

Besides the discharge products composition, there is an important difference in the minimum discharge time necessary for detection of the species. In the cycle with de iodide some discharge product is already formed in the first two hours, while without it only after 4h there was some indication of product being formed, and still, this peak is discreet comparing to the first mentioned. Thus, we can say that either the formation of discharge products in the presence of LiI happened significantly faster than the non-mediated one or the LiOH formed in the presence of I^- is arranged in a higher degree of crystallinity.

The use of $LiNO_3$ on Li-O_2 batteries is known for Li^+ and NO_3^- ions interactions with superoxide and peroxide anionic species in solution phase allowing the formation of large toroidal-shaped Li-peroxide deposits, that differs from the typical Li_2O_2 morphology. The articles that investigate LiI's addition into the system usually focus on its effects on the charge step of the cycle, which is probably the reason why any reports on iodide affecting the ORR kinetics couldn't be found.

CHAPTER 6

Operando Synchrotron XRD Characterization of Li-O_2 Batteries with LiBr as Redox Mediator

6. *Operando* synchrotron XRD characterization of Li-O_2 batteries with LiBr as redox mediator: Publication III

6.1 Introduction

In a scenario of growing environmental awareness, the development of cleaner energy supplies has been presenting as a key factor towards a more sustainable matrix. For energy storage systems the Li-ion batteries have been one of the most used and reliable for the past years, however, the desire for higher energy densities has led researchers to look beyond Li-ion for future applications. In this context, Li-O_2 has emerged as a possible technology, with the potential to deliver 5-10 times the specific energy density of Li-ion (LANDA-MEDRANO et al., 2019). In aprotic Li-O_2 cells, ideally, during discharge, molecular oxygen is reduced via the oxygen reduction reaction (ORR) to form oxidized lithium species - such as LiO_2, Li_2O and $Li_{i2}O_2$ - on the cathode. This process might also yield to LiOH or other species if small amounts of dissolved water are in the aprotic media, which might be easy to control under lab conditions, but impose a complex control for a potential device manufacture. During charge the process is reversed and the discharge products are decomposed and oxygen is released via the oxygen evolution reaction (OER) (GIRISHKUMAR et al., 2010).

The insoluble and nonconductive nature of Li_2O_2, the discharge product expected to be mostly formed, requires the application of a high potential for its oxidation to happen. This high overpotential during charging promotes side reactions, such as electrolyte and electrode degradation, which leads to low cyclability and low energy efficiency. These are some of the many challenges that remain even after years of study (LIU et al., 2017c). To overcome this issue, a more efficient oxidation route for Li_2O_2 has been proposed by the use of redox mediators (RMs) (KWAK et al., 2018). This class of compounds are basically soluble catalysts that are dissolved in the electrolyte and participate of the reaction as energy carriers. During the RM-assisted charge the mediator is electrochemically oxidized at the electrode's surface which subsequently oxidizes Li_2O_2 chemically (KO et al., 2019). The transformation of the charge reaction from electrochemical to chemical, reduces the formation of highly reactive intermediates upon electro-oxidation of lithium peroxide, and reduces the charge overpotential. The majority

of the RMs can be classified into three categories: organic, organometallic and halides (PARK et al., 2018).

There has been several important published works related to the use of some redox mediator molecules in Li-O_2 system, mostly organic (CHEN et al., 2013; QIAO; YE, 2016; GAO et al., 2017), organometallic (RYU et al., 2016; KWAK et al., 2018), and inorganic halides such as LiBr (KWAK et al., 2016; LEE; PARK, 2016; LIANG; LU, 2016; LEE; KWAK; SUN, 2017; XIN; ITO; KUBO, 2017) and LiI (LIM et al., 2014; KWAK et al., 2015; BURKE et al., 2016; QIAO et al., 2017; TUŁODZIECKI et al., 2017). However, all cited studies have been made on cells with low or very low loadings for active materials which have more accessible surface area and better normalized discharge capacity. Despite the promising results, a question remains: can those reported solutions for better charging be successfully applied into a more complex, highly porous and with higher loading electrodes? This question is crucial for understanding if this technology will be able to provide a robust solution for a potential practical Li-O_2 cell as mass transport interplay for the RMs has not yet been discussed.

From the prospects of RM candidates, organic mediators have been associated with intrinsic instability when operating in the wide potential domains upon any practical operation of Li-O_2 batteries (PARK et al., 2018); LiI-mediated cells have been related with the promotion of side reactions with ether-based electrolyte solutions and with impurities, lowering its importance. LiBr has been considered as an interesting RM, yet it was recently identified as a corrosive additive (in the form of Br_3^- and Br_2) during prolonged operation of Li-O_2 cells (KWAK et al., 2018). Among all the reported RM species, the last is the least studied so far, being most of studies with glyme based electrolytes (KWAK et al., 2016; LEE; PARK, 2016; LIANG; LU, 2016; XIN; ITO; KUBO, 2017), so further investigation for a better understanding is needed.

In this study we use operando XRD characterization from a synchrotron light source. Our objective is to understand the effect of RMs addition, specifically, LiBr on the non-aqueous Li-O_2 system with a highly porous electrode based on MWCNT with higher loading and surface area (around 10 times higher than most of previous studies) (KWAK et al., 2016; LEE; KWAK; SUN, 2017). With that we aim to elucidate the Li_2O_2 formation and decomposition as a function of the discharge and charge capacity. We also provide an investigation over the discharge products and the effect of residual water in the system when exploring a DMSO based device in conjunction with LiBr. We show here how DMSO-based cells leave the system more exposed to water contamination,

leading to LiOH formation, which is not observed in glyme-based studies (KWAK et al., 2015; LIU et al., 2015). In terms of cell limitation, using electrodes with active material masses substantially higher than most of the studies in this area, we verified that LiBr has responded catalytically as expected according to literature. However, cell "sudden death" caused by clogging after 37 cycles indicated that under some conditions the system's issue move from catalytic to mass transfer, imposing novel challenges for the Li-O_2 community.

6.2 Methods

6.2.1. Gas diffusion electrodes synthesis

The method for electrodes preparation were the same as the one described in the previous chapter. Electrodes with masses on the range 3.00 ± 0.1 mg were selected for testing in this study.

6.2.2. Cell assembly and electrochemical studies

Dimethyl sulfoxide (DMSO) (Sigma Aldrich, 99.99% anhydrous), the aprotic solvent used, was dried using molecular sieves (3 A, Sigma Aldrich) on the electrolyte with LiBr as redox mediator. Electrolyte solutions consisted of 0.1 M $LiClO_4$ (Sigma Aldrich, 99.999% anhydrous) in DMSO and the second, this same solution with the addition of 50 mM LiBr (Sigma Aldrich, 99.99%). A metallic lithium disc (Tob Machine, 99.99%) was used as the cell's anode. All the described materials were exposed only to argon atmosphere.

Assembly, cycling and *operando* XRD characterization tests took place and were performed just as described in the previous chapter.

The tests were performed in two electrolyte and electrode conditions: in the first condition solvent and CNT electrode did not go through drying step; in the second molecular sieves were added to the solvent 72 h prior to electrolyte solution preparation and the CNT based electrodes were dried in oven for 2h at 105 ºC and transported to the glovebox antechamber in a desiccator to allow minimum contact with humid air.

6.2.3. Battery cycling

Before non-*operando* cycling, the cells where purged with O_2 for 10 minutes at a flow rate of 0.3 $L.min^{-1}$ in OCP. Discharge-charge tests were capacity limited and carried out galvanostatically with a 33.3 mAg^{-1} current density (with a negative current causing discharge and a positive current causing charge) on a potential window from 2.4 to 4.1 V. After cycling, cells were purged with N_2 and opened inside the glovebox to prevent electrode contact with the air and contamination. Samples were kept in the inert environment until subjected to further characterization.

6.2.4. *Ex situ* characterization

Electrodes were investigated using Renishaw inVia Raman spectroscope with He-Ne 632.8 nm (1.96 eV). T Spectra were measured at room temperature using a 50X objective lens and Raman Shift was calibrated using the instrument internal silica positioned at 520.6 cm^{-1}. Spectra analyses were accomplished by proper subtraction of the baseline, deconvolution using Lorentzian distribution functions, and normalization by intensity of the G band obtained for each spectrum. The electrodes subjected to Raman spectroscopy characterization were placed on the El Cell® Opto Std cell inside the glovebox and sealed to be analyzed without any contamination. A Sapphire window, was used on the cell.

The surface morphology of the scaffold was examined using a FEI high speed Inspect F50 scanning electron microscope at the Brazilian Nanotechnology National Laboratory (LNNano).

6.3 Results and discussion

The synthesized electrodes for this study were initially characterized by SEM and Raman spectroscopy (Figure 23 a and b, and c, respectively). SEM evidenced the MWCNT growth over the stainless steel with a radial distribution covering the entire surface as previously reported (CARVALHO et al., 2019). A typical Raman spectra for carbon nanotubes are also evidenced by the presence of D, G, D' and G' bands at ~1352 cm^{-1}, ~1582 cm^{-1}, ~1600 cm^{-1} and G' ~2700 cm^{-1}, respectively (LOBO et al.,

2005). These electrodes were used without further modifications as the working electrodes for all the following tests with and without the drying step for each analysis

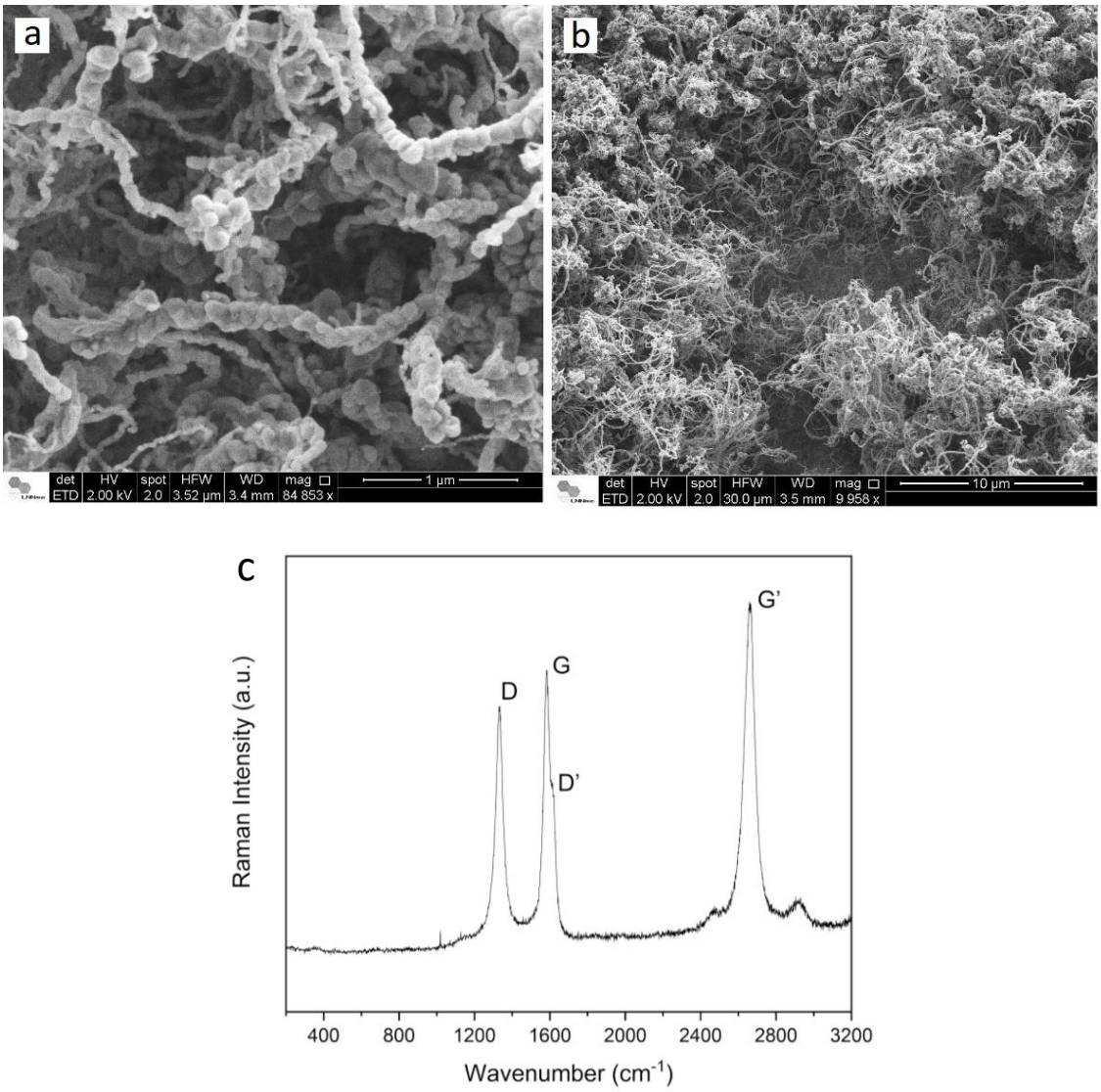

Figure 23: a and b) SEM images of pristine electrodes; c) Raman spectra of the pristine electrode.

6.3.1 Residual water influence

Aprotic solvents often contain residual water and completely removing it might impose a technological challenge for future manufacture and severe restriction regarding the O_2 to be supplied. Therefore, we first investigated the residual water influence over the discharge reaction using the non-dried electrolyte and electrode for a Li-O_2 cell and to better understand the effects of subsequently adding LiBr into the system. *Operando*

XRD characterization of the described Li-O_2 cell (Figure 24 a) shows the diffractograms of the electrodes as it discharged progressively. The broad diffraction peak at 2θ ≅ 40.9° is related to MWCNT of the electrode grid and it will be present in all XRD studies of this work. Lithium peroxide (Li_2O_2, JCPDS n° 09-0355) reflection peak around 40º did not pronounce sharply, but by broadening the MWCNT peak. The broad and low intense peak exhibit at ≈37.9° correspond to the (101) plane of hexagonal crystalline phase of Li_2O_2. Nevertheless, after 15h of discharge, the carbon diffraction peak showed an asymmetry. This can be correlated to the increase of the Li_2O_2 diffraction peak at 40°, once that the most intense peak of this lithium specie (at ≈ 37.9°) has become more intense.

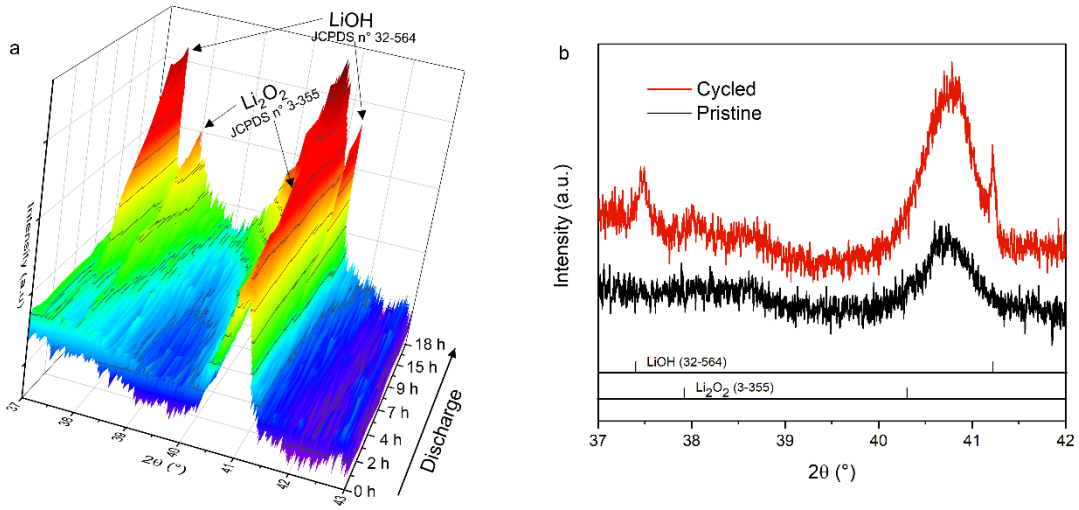

Figure 24: a) *Operando* X-ray diffraction patterns of Li-O_2 cell without LiBr as redox mediator, current density fixed at 33.3 mAg^{-1}; b) *ex situ* XRD pattern of electrode discharged with LiBr at a current of 33.3 mAg^{-1}.

Diffraction peaks at ≈ 37.5º and ≈ 41.3º correspond to lithium hydroxide (LiOH, JCPDS n° 32-0564), which are attributed to (101) and (110) planes of the tetragonal structure, respectively. We can see an increase on the intensity of the XRD peaks of both LiOH and Li_2O_2 with the increase of the discharge capacity. Since electrode and electrolyte had not been dried prior to cell assembly, the discharge products led us to imply that the water present, determined by Karl Fisher titration, was most likely to be available on the system, allowing Li^+ to react with both O_2 and H_2O, by the reactions on Equation 21 and 22, respectively. The LiOH formation by reaction between Li_2O_2 and H_2O (Equation 23) is also reported by some authors (ZHANG; ZHOU, 2013; GUO et al., 2014).

$$2Li^+ + 2e^- + O_2 \rightarrow Li_2O_2 \quad (21)$$

$$4Li^+ + 4e^- + 2H_2O + O_2 \rightarrow 4LiOH \quad (22)$$

$$2Li_2O_2 + 2H_2O \rightarrow 4LiOH + O_2 \quad (23)$$

Cells were subsequently assembled with the electrolyte containing LiBr mediator, and herein the system was still non-dried. Figure 24 b presents *ex situ* XRD data of the electrode after discharge. It clearly reveals the formation of the same products observed during *operando* XRD cycling (Figure 24 a), so the addition of LiBr did not favor the formation of a specific product during discharge, meaning that the reaction route was not altered by the mediator's presence.

Kwak and coworkers (2016) studied Li-O_2 cells in the presence of LiBr and LI with the addition of water. Their results indicate that with 1000 ppm of water in the systems only the iodide mediated cell presented LiOH in the XRD peaks, which had been previously reported (KWAK et al., 2015; LIU et al., 2015). In the bromide system, the discharged cathode exhibited peaks characteristic for crystalline Li_2O_2 exclusively. Schwenke and coworkers (SCHWENKE et al., 2015) assessed the effect of water on the lithium peroxide yield (in the absence of RMs) and also found evidence of Li_2O_2 as the main discharge product, even in the presence of substantial amounts of water, and no significant amounts of LiOH and LiOH·H_2O were produced. Both studies differ from the results we present here.

Karl Fischer titration method indicated that the electrolyte we used on the cells was prepared with DMSO with a water content of 108 ± 4 ppm. Even with a concentration almost 10 times lower than the one in the Kwak and coworkers' study, LiOH was formed. The mentioned studies, however, were tetraglyme based, with LiTFSI.

Some studies have identified that Li^+ cation's solvation by solvent molecules or salt anions is a major factor in the reaction mechanism (GITTLESON et al., 2017; LYU et al., 2017). According to Lyu and co-workers (2017), lithium perchlorate ($LiClO_4$) and lithium bromide (LiBr) mainly formed Li_2O_2 and showed the best stability when comparing to other salt anions such as lithium hexafluorophosphate ($LiPF_6$), lithium trifluoromethanesulfonate (LiTf), lithium bis(trifluoro-methanesulfonyl)imide (LiTFSI) and some others (LYU et al., 2017). Nevertheless, even using $LiClO_4$ and LiBr in the electrolyte, LiOH was still produced. Regarding the solvent, comparing DMSO and the glymes, despite DMSO having a higher donor number (DN), which is commonly associated with a better stability for the superoxide intermediate in the peroxide reaction

route, the tetraglyme (TEGDME) molecule interaction with Li^+ ion is stronger. While DMSO has only one oxygen atom, TEGDME has five, which means that in some conditions, each Li^+ can be solvated by a single solvent molecule, almost in a circular way (AGUILERA et al., 2015), therefore shielding it from water reaction. Computational simulation has shown that TEGDME protects Li+ better than DMSO, letting the ion less available to react with any water content on the system. These interactions can lead us to a better understanding on why the DMSO-based system presented here had LiOH as product, even with a water content significantly lower than previous studies, and more importantly, elucidates that the LiBr does not play any role on discharge mechanism.

6.3.2 *Operando* characterization of LiBr mediated Li-O_2 cells

Hereafter studies were carried with the dried electrodes and electrolyte solution, we tested the same system after removing all residual water, according to the described methods. Our electrodes had a much higher material loading and overall surface area than previous studies (KWAK et al., 2016; LEE; KWAK; SUN, 2017), which could impose an addition challenge for the charging assisted mediated mechanism as the activated Br_3^- species must reach all formed Li_2O_2. To track the reaction progress towards formation and decomposition we used XRD *operando* characterization over a complete discharge/charge cycle in a Li-O_2 cell with LiBr (Figure 25 a). In this experiment, we used a lower capacity of 260 $mAh.g^{-1}$ due to the long time required in the synchrotron facility. To better track the products evolution, we also performed a single discharge to a higher capacity (Figure 25 b). We can identify the process of Li_2O_2 formation, while LiOH peaks are not present in this system, confirming that this last specie indeed derived from the reaction of Li^+ and/or Li_2O_2 with the water present in the cell.

During the discharge process, the diffraction peaks related to Li_2O_2 crystalline phase, progressively increased up to 7h. This revels that, in the presence of LiBr, Li_2O_2 nanocrystals starts being formed between two and three hours after the beginning of discharge or that only after that time the electrode accumulated the lowest detectable amount of the discharge product. The 2D contour surface maps (Figure 25 a and b, left) clearly show the enlargement of the diffraction peak located at $2\theta \approx 40.9°$, which is related to MWCNT, due to the lithium peroxide product formation. Moreover, the products decomposition was also evidenced.

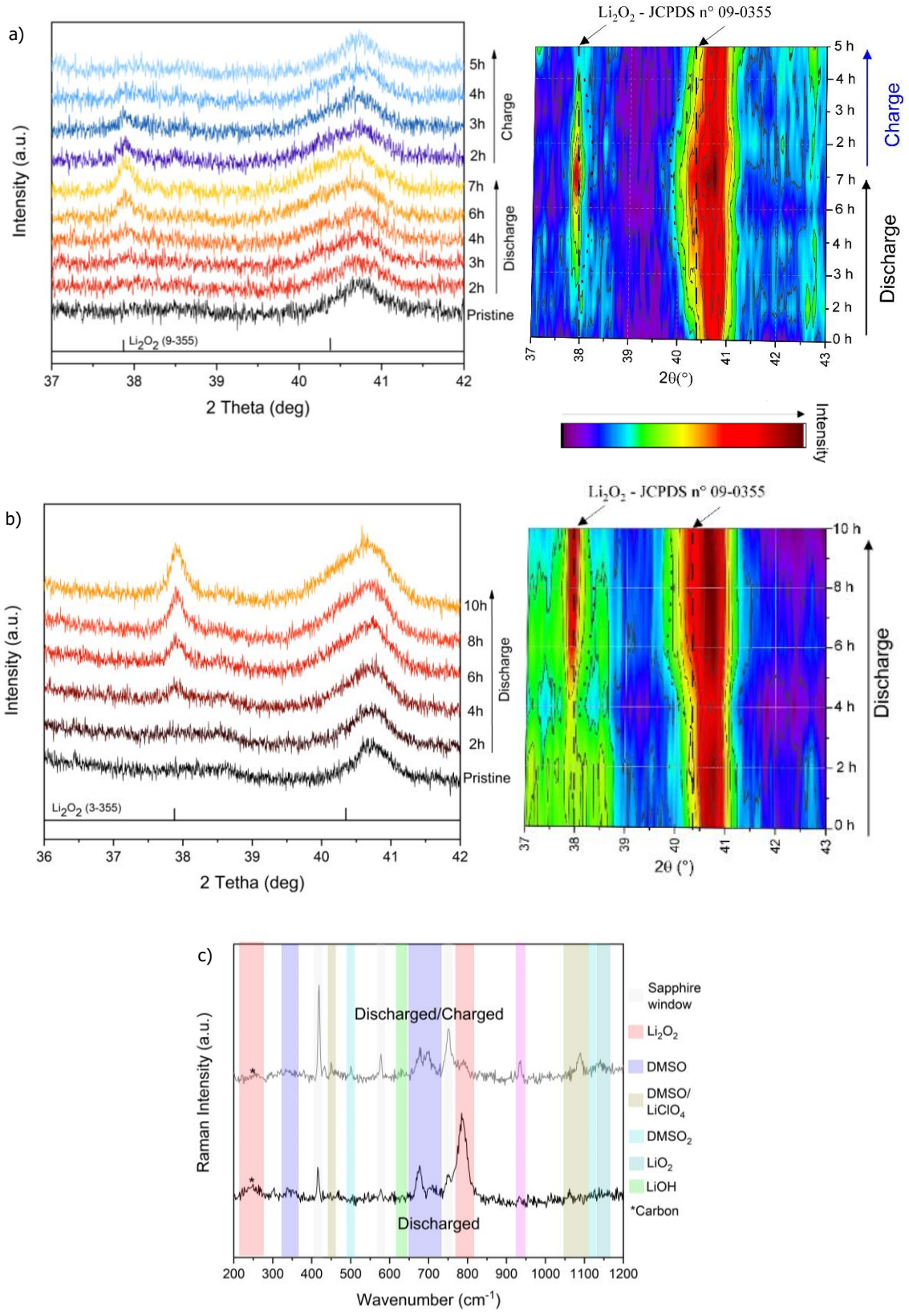

Figure 25: *Operando* XRD characterization of Li-O_2 cells with LiBr as redox mediator assembled with Electrodes a) after full cycle and b) after discharge; c) Raman shifts of electrodes after discharge and full cycle (discharged/charged).

After the *operando* XRD measurements, all electrodes were stored inside of the glove box and subsequently subjected to Raman spectroscopy. Raman shifts are shown in Figure 25 c. Li_2O_2 discharge product was identified by this technique in both Electrodes. After charge, Li_2O_2 bands intensities were significantly lower than after discharge. Considering that these electrodes, when as prepared, had sufficient similar characteristics and were used for cell assembly and cycling at very similar conditions, we can see the reduction on Raman bands as a confirmation of an effective peroxide decomposition with the charge process.

The Raman band located at 1140 cm^{-1} in the discharged/charged profile refers to O-O stretch of LiO_2 (PENG et al., 2011), which is soluble in DMSO (WANG et al., 2020). We propose that LiO_2 was formed during charge due to interaction with Br_3^-, analogous to the process described by other authors (WANG et al., 2018, 2020). Due to the high donor number (DN = 29.8) of this solvent it has the ability to stabilize and liberate lithium superoxide during the OER (ABRAHAM, 2015). As recently reported, the anion shape and DN of lithium salts have a high impact in the Li^+ solvation (FIATES et al., 2020). The Br^- also has high donor number (DN = 32.3 in DMSO) (LINERT; JAMERSON; TAHA, 1993) and could partially solvate the Li^+ and influence in the intermediary species. Moreover, during a LiBr-assisted charge process, the interaction with Br^-/Br_3^- redox couple is expected, as shown in Equation 24 and 25 (LIANG; LU, 2016).

$$3Br^- \leftrightarrow Br_3^- + 2e^- \quad (24)$$

$$Li_2O_2 + Br_3^- \rightarrow 2Li^+ + O_2 + 3Br^- \quad (25)$$

However, if the incomplete Li_2O_2 decomposition by LiBr redox mediator occurs during the charge process, lithium superoxide is formed. The small bands located at ~500 and ~1125 cm^{-1} are related to the dimethyl sulfone, which is formed as a result of Li_2O_2 interaction with DMSO (MOZHZHUKHINA; MÉNDEZ DE LEO; CALVO, 2013). The presence of LiOH, also a product of the chemical reaction between the DMSO and the Li_2O_2, is evidenced by the band at 620 cm^{-1} (HARBACH; FISCHER, 1975; GITTLESON et al., 2015). This chemical reaction has been reported in other studies (MOZHZHUKHINA; MÉNDEZ DE LEO; CALVO, 2013; SHARON et al., 2013; SCHROEDER et al., 2015). The fact that the electrochemical window used in this study is withing the DMSO electrochemical stability range (READ, 2002; MOZHZHUKHINA;

MÉNDEZ DE LEO; CALVO, 2013) strengthens our hypothesis that these by-products are a result of chemical reactions not electrochemical decomposition of the electrolyte.

The other bands correspond to species that are components of the cell, such as DMSO and $LiClO_4$. Analyzing the results obtained on the very same electrodes provided by two techniques, Raman spectroscopy confirmed the species shown on the XRD patterns. From this result we can either conclude that on the last XRD charge pattern there was not sufficient Li_2O_2 to be detected or that crystalline Li_2O_2 was firstly decomposed and some non-crystalline phase remained and could be identified spectroscopically. The electrodes were then subjected to SEM analysis and the images are presented in Figure 26.

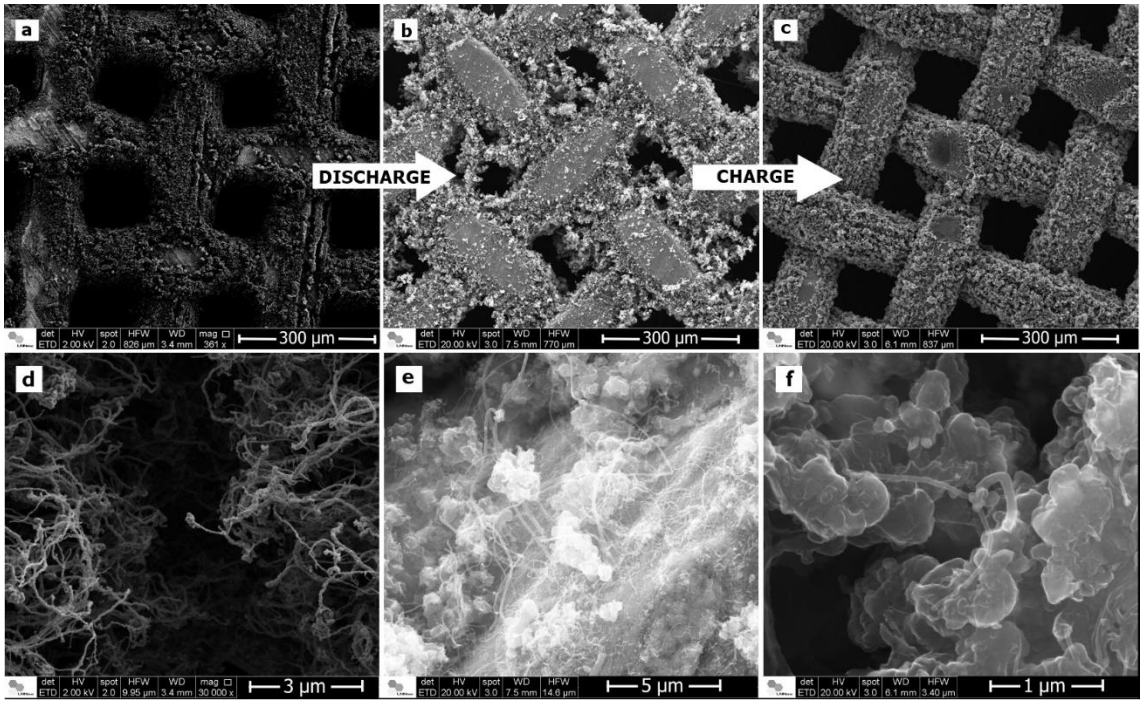

Figure 26: Scanning electron microscopy images of a) Pristine electrode (HFW,mag=361x); b) Electrode 1 – discharged (mag=348 x); c) Electrode 2 – discharged and charged (mag=353 x); d) inset of the pristine electrode (mag=30 kx); e) inset of Electrode 1 – discharged (mag=17.8 kx); f) inset of Electrode 2 – discharged and charged (mag=85 kx)

From Fig. 26 a to b we can see that the discharged electrode shows the mesh being filled and its morphology modified by the presence of some deposited material on the surface. From Fig. 26 b to c, the solid material had been decomposed partially during charge, with the electrode surface retrieving a morphology similar to the pristine electrode shown on Fig. 26 a. For a first cycle, which did not reach extreme conditions, such as a low cell voltage or a very high discharge capacity, it is reasonable to accept that the

electrode had restored not completely, but substantially its initial condition. From the microscopy images with larger magnification (Figure 26 d-f) the nanotubes and the discharge product can be clearly seen. Comparing Figure 26 f (discharged and charged) with 26 d (pristine), the presence of deposits confirms that not all the products had been decomposed during charge. This evidence is also in agreement with the discussed Raman results showing residual Li_2O_2 (Figure 26 c) and LiO_2.

6.3.3 Cycling tests

Redox mediators have been reported as promising solutions to improve not only the high charging plateaus in Li-O_2 cells, but mainly their cyclability by the chemical decomposition of the discharge products through the oxidized (activated) soluble mediator. To identify the effect of LiBr as RM in our porous MWCNT based electrode, cells were assembled and cycled with and without LiBr for comparison. Figure 27 presents the galvanostatic cycling test profiles, different potential cut offs were set for each system due to a significant lower charging plateau from the mediated cell.

Figure 27 a and b shows cycling profiles to 500 $mAh.g^{-1}$, being the first without the redox mediator and the last, with LiBr. Figure 27 c and 27 d shows the profiles with capacities limited to 116 and 50 $mAh.g^{-1}$, respectively. Comparing the cycling profiles of the cells limited to the same capacity, we can note that for the discharge process the cell potential was essentially the same. However, as expected, for the mediated cell the charge plateau was considerably lower.

For the non-mediated cycling, in our highly porous electrodes, we can see that the charge plateau reached the 4.5 V vs Li/Li^+ cut-off at the second charging cycle, in fact, from the first charging cycle this system exhibited a high overpotential falling into the range reported for DMSO decomposition (MOZHZHUKHINA; MÉNDEZ DE LEO; CALVO, 2013). This fact indicates that some degradation process might occur promoting the formation of irreversible by-products and emphasize the challenge of creating highly porous electrodes for Li-O_2 cells. The sharp increase on the overpotential at the second charge endorses the hypothesis of a resistive material formation on the previous discharge, preventing further cycling.

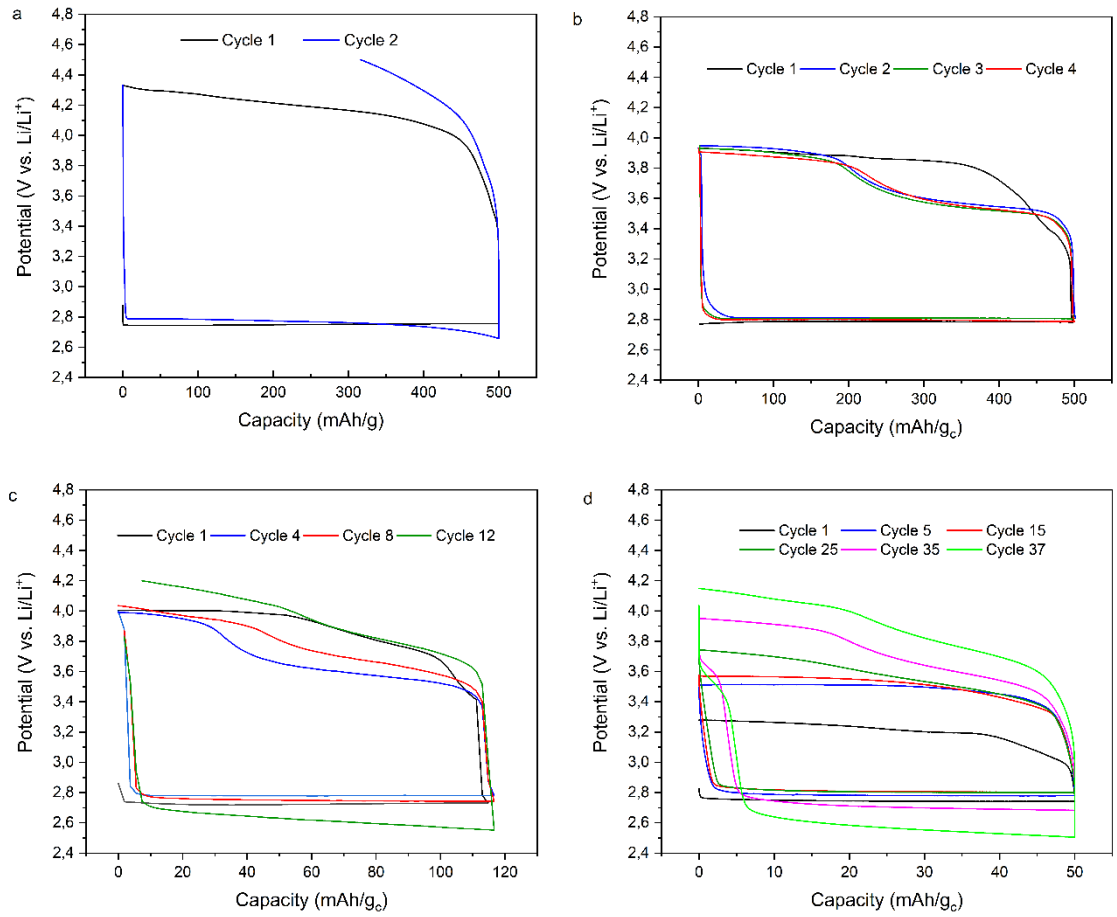

Figure 27: Electrochemical cycling profiles of Li-O_2 batteries a) without redox mediator and capacity limited to 500 mAh.g^{-1}; with LiBr and capacity limited to b) 500 mAh.g^{-1}; c) 116 mAh.g^{-1}; d) 50 mAh.g^{-1}

An O_2 saturated electrolyte in the presence of LiBr usually presents two reversible redox reactions, involving the Br^-/Br_3^- and Br_3^-/Br_2 couples. The equilibrium voltages for these reactions depend on the system's electrolyte, as the solvent energy, which is solvent-dependent, will influence the reversible potential (LIANG; LU, 2016). For LiBr and DMSO as solvent, Lee et al. (LEE; KWAK; SUN, 2017) have shown that the reduction and oxidation peaks are around 3.5 and 3.72 V vs Li/Li$^+$.

The charge profiles of the system with RM had a quite different behavior from the ones without it. Mediated charge started at much lower overpotentials ~ 3.5 V vs Li/Li$^+$ after the first cycle, consistent with previous results that confirm the activity of LiBr on the peroxide oxidation reaction (KWAK et al., 2016; LIANG; LU, 2016; LEE; KWAK; SUN, 2017; XIN; ITO; KUBO, 2017). The charging plateau happened in 2 steps, the first around 3.5 V and the second plateau just under 4.0 V vs Li/Li$^+$. This result is consistent with the electrochemical oxidation of Br^- to form Br_3^- and then oxidize Li_2O_2,

releasing Li^+, O_2 and Br^- (KWAK et al., 2016). This behavior was also seen when limiting the cell capacity to 116 $mAhg^{-1}$ and to 50 $mAhg^{-1}$, although a higher number of cycles were needed to exhibit the same charge pattern.

Kwak and co-workers (KWAK et al., 2016) suggest that the shape of the charging voltage profiles is a consequence of the Br^- oxidation kinetics on the carbon cathode. After the discharge process, the cathode is covered by a non-conductive Li_2O_2 layer. During charge, Br^- needs free sites on the carbon cathode to be oxidized to Br_3^-. They proposed a higher concentration of LiBr (1 M) to increase the chance for Br^- oxidation, even when the electrodes are extensively covered by Li-peroxide. Our electrolyte contains a LiBr concentration similar to that study and the cycling profiles here are consistent with the ones obtained there, endorsing the hypothesis brought by the authors. The first charge plateaus observed on Figure 27 b and c present higher overpotentials than the subsequent ones. It can be because on the first discharge Li_2O_2 is formed more uniformly, with no preferential sites for its growth, leaving few sites for the reaction from Br^- to Br_3^-. On the following cycles, however, the insoluble product might not have been totally decomposed on the previous charge, as shown by the Raman and SEM results, allowing the formation of preferential sites for Li-peroxide growth. This leaves more sites with no deposit available for Br^- to be oxidized from the second cycle forward. Cycling from the Figure 28 d differs from the previous, since the limited capacity on this test was so small it was not enough to cover all the active sites leaving free surface for Br^- oxidation since the 1^{st} cycle.

After several cycles, however, an opposite trend was observed. The overpotential for charging continuously increased, as seen in cycles 8^{th} – 12^{th} (Figure 27 c) and 15^{th}-37^{th} (Figure 27 d), which indicate that the residual undecomposed Li_2O_2, as seen by Raman and SEM, can easily accumulate in highly porous electrodes or in electrodes with higher loadings as our case. This in turn will lessen the free sites for Br^- oxidation which can accentuate the concentration gradients cycle after cycle, resulting in the seen higher overpotentials for higher cycles. Therefore, mass transfer limitation for the pair Br^-/Br_3^- might be responsible for the increasing inefficiency in this cell, as we expect no change in the activation energy for the redox pair over the carbon surface. Raman analysis confirms that the high-donicity of the electrolyte composed by Br^- and DMSO solvent favors the formation of LiO_2 during the charge process, which also could contribute for the short cycling life of lithium-air batteries (WANG et al., 2020).

To endorse the significance of mass transfer influence in this system, we present in Figure 28 a direct comparison of second to fourth charge profiles as a function of the percentual of total charge capacity, in 116 and 500 $mAhg_c^{-1}$ limited cycles. We observe that the changing points from first to second plateaus are within the range of around 50 to 70 % of the total capacity, regardless of the actual cell capacity and therefore, from the overall amount of Li_2O_2 still to be decomposed. Considering that, from the second cycle forward the electrode had free site for the Br^- oxidation, the smooth linear increase in the charging potential around 3.5 V, and the subsequent change in the plateau to 3.8-4.0 V, are the effect of mass transfer polarization. Mass transfer starts to limit the cell as the rate of Br_3^- formation exceeds the rate of Br_3^- reaction with Li_2O_2, creating concentration gradients for Br^- and Br_3^-. Once the concentration of Br^- is substantially diminished, the system starts to further oxidize the Br_3^- to Br_2, and a new charging plateau is formed.

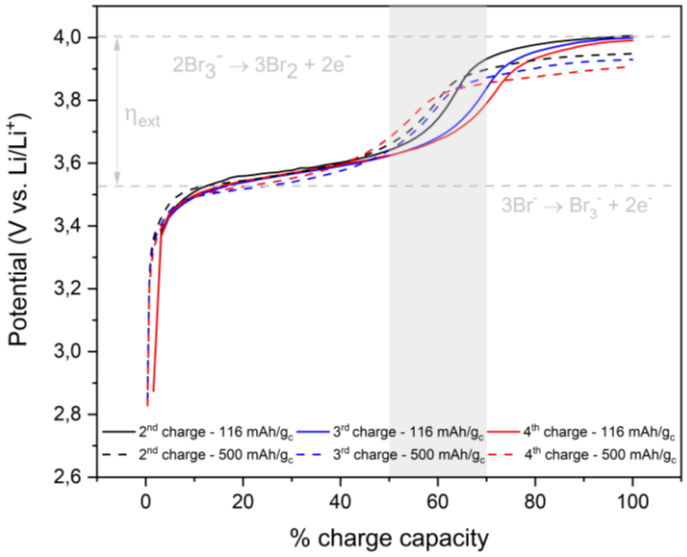

Figure 28: Charge profiles against % of total charge capacity of the cycle. The arrow indicates the extra overpotential (η_{ext}) from the first plateau to the second.

In electrodes with not so readily accessible surface and/or tortuous paths, as our case, the Br_3^- transport from the free sites to the Li_2O_2 starts to be difficulted by the decrease of available Li_2O_2. This decrease, however, seems not to be directly correlated to the overall amount of Li_2O_2 left in the electrode. This is more evident as mass transfer limitation started acting towards the establishment of the new plateau slightly before in the 500 $mAhg_c^{-1}$ limited system, despite the higher amount of Li_2O_2 still present. Li_2O_2 crystals continuously nucleates, forming more of them as the cell discharge increase.

When the mediated charge proceeds, the Br_3^-/Li_2O_2 reaction is facilitated around the larger crystals (Figure 26 b), but when those diminish, Br_3^- cannot easily access the crystals that are entangled within the MWCNT structure. This conclusion is also in agreement with the SEM (Figure 26 f) which shows still some solid products around the CNT structure without any lager crystals on top bringing mass transfer again as an important limitation to this system emphasizing the importance of the cathode architecture for efficient Li-O_2 batteries.

Cells exhibited a stable discharge capacity during the first cycles, with discharge plateaus around 2.75 V. On the cycling limited to 50 $mAh.g^{-1}$ the plateaus only decreased significantly after 30 cycles, indicating that an amount of discharge products was accumulated on the cathode surface, becoming a real burden to the system on this stage. Figure 29 shows a micrograph of the electrode which cycling profile is shown on Figure 27 d. It is clear that the electrode's 3D network had been almost completely clogged, hindering oxygen diffusion, covering free sites for the Br^- oxidation, and making the system very resistive for the process. This result corroborates with the cycling profiles relating to the Br^- oxidation kinetics on the carbon cathode (KWAK et al., 2016). At some stage, the amount of accumulated discharge products prevents the bromide oxidation and current flow. According to Viswanathan and coworkers (2011), Li_2O_2 stops being formed when the current through the insulating Li_2O_2 layer no longer allows the electrochemical current flow, causing the cell "sudden death", It was exactly what happened right on the cycle subsequent to the 37^{th} shown on the cycling profile (Figure 27 d).

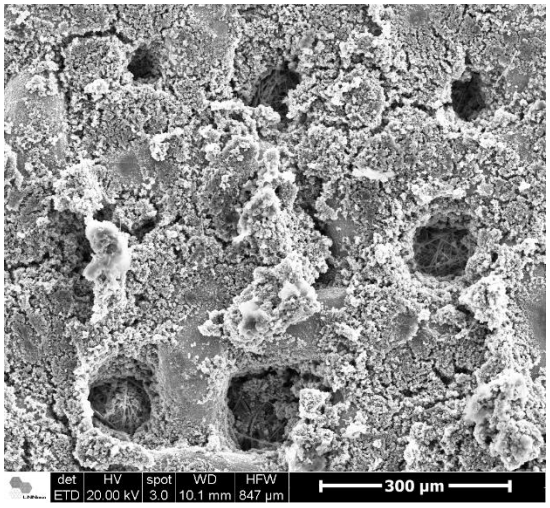

Figure 29: Scanning electron microscopy image of an electrode after 37 cycles.

6.4 Conclusion

In summary, this study approaches the Li-O_2 system in cell and cathode configuration, Swagelok cell and high load electrode, substantially closer to a possible viable prototype than most of studies in this area. Our results confirm that LiBr as redox mediator do contribute to unravel the system's catalysis issue, however regarding the development of a cell more similar to practical devices, there are still challenges to be surpassed. We show here that in the case of LiBr, despite de charge overpotential reduction, profiles of cycling with electrodes with a high active material mass indicate significant accumulation of insoluble products on its surface, moving the issue from catalytic to mass transfer. This result emphasizes the need for more effort towards improving the cell design and electrode material and architecture in order for us to move in the direction of reaching viable devices.

7. Final Considerations

Synchrotron FTIR and XRD techniques were used to characterize Li-O_2 and Li-Air systems in time-resolved mode. For both studies, new cell designs were created and used for each technique. The main challenge surpassed in the cells design was comprise the cells minimum requirements for operation and the technique's operational limits, since in many points the requirement of the Li-O_2 technique was exactly a technique limitation, leaving a very tine line of possibilities for us to work with - specially with the SINS technique.

For the infrared spectrum region study, micro-FTIR and SINS spectroscopies were used. Despite the significant difference in the discharge rate used the detected discharge products were the same. In addition to that, we were able to identify formate species being formed and electrolyte degradation after a very short discharge time, 140 s, due to interaction with Li_2O_2 formed. The findings revealed by this study emphasizes both techniques relevance in the investigation complex processes typically found in conversion batteries.

With the XRD studies we were able to better investigate the effect redox mediators to Li-O_2 cells, more deeply, using *operando* methodology with LiBr. In the bromide mediated system, we assessed the influence of residual water presence in the cell and verified that in DMSO-based systems, even with very low water content, LiOH is formed. We also have observed that, despite the substantial overpotential reduction, bromide-mediated batteries with a high loading active material electrode still faces significant limitations, as we saw significant accumulation of insoluble products on the electrode surface, indicating a transition of the issue from catalytic to mass transfer. This indicates that the development of viable devices still faces important challenges, despite the great improvement brought by the redox mediators' addition to this technology.

8. Suggestions for future work

Due to the consequences of the COVID-19 pandemic, a significant portion of the experimental activities planned for this doctoral thesis projects could not be carried out. Based on the key issues that could not be included in the research, I bring the following suggestions for future work:

1. Rotating disc electrode (RDE) study – conduct a full fundamental electrochemistry study with the RMs used here with the electrolytes mostly used by our group. The sealed three-electrode cell necessary for this study was designed by the group and was recently ready. It is currently under testing for validation.
2. Investigation of redox-mediated cells with the micro-FTIR technique in *operando* mode – based on Chapter 4 findings, micro-FTIR technique has an important the applicability to study complex processes as the ones involved in the Li-O_2 cell. An electrochemical device for multi-technique chemical characterization of electrodes in *operando* mode was designed by the group. Among the characterization techniques for which it can be used is the FTIR. With this new cell and this technique applicability to study the system, the effect of RM addition to the Li-O_2 batteries can be significantly unveiled.

9. References

ABRAHAM, K. M. Electrolyte-Directed Reactions of the Oxygen Electrode in Lithium-Air Batteries. **Journal of The Electrochemical Society**, v. 162, n. 2, p. A3021–A3031, 2015.

ABRAHAM, K. M.; JIANG, Z. A Polymer Electrolyte − Based Rechargeable Lithium / Oxygen Battery. **Journal of the Electrochemical Society**, v. 143, n. 1, p. 1–5, 1996.

AGUILERA, L. et al. A structural study of LiTFSI – tetraglyme mixtures : From diluted solutions to solvated ionic liquids A structural study of LiTFSI – tetraglyme mixtures : From diluted solutions to solvated ionic liquids. **Journal of Molecular Liquids**, v. 210, n. May, p. 238–242, 2015. Disponível em: <http://dx.doi.org/10.1016/j.molliq.2015.04.053>.

AURBACH, D. et al. On the Surface Chemical Aspects of Very High Energy Density, Rechargeable Li–Sulfur Batteries. **Journal of The Electrochemical Society**, v. 156, n. 8, p. A694, 2009.

BEATTIE, S. D.; MANOLESCU, D. M.; BLAIR, S. L. High-Capacity Lithium–Air Cathodes. **Journal of The Electrochemical Society**, v. 156, n. 1, p. A44, 2009. Disponível em: <http://jes.ecsdl.org/cgi/doi/10.1149/1.3005989>.

BRUCE, P. G. et al. Li–O2 and Li–S batteries with high energy storage. **Nature Materials**, v. 11, n. 02, p. 172–172, 2012.

BURKE, C. M. et al. Implications of 4 e- Oxygen Reduction via Iodide Redox Mediation in Li-O2 Batteries. **ACS Energy Letters**, v. 1, n. 4, p. 747–756, 2016.

CARVALHO, V. S. et al. Radially ordered carbon nanotubes performance for Li-O2 batteries: Pre-treatment influence on capacity and discharge products. **Catalysis Today**, n. September, p. 0–1, 2019. Disponível em: <https://doi.org/10.1016/j.cattod.2019.09.030>.

CHEN, Y. et al. Charging a Li-O2 battery using a redox mediator. **Nature Chemistry**, v. 5, n. 6, p. 489–494, 2013.

CHOI, N. S. et al. **Protective layer with oligo(ethylene glycol) borate anion receptor for lithium metal electrode stabilizationElectrochemistry Communications**, 2004. .

CHRISTENSEN, J. et al. A Critical Review of Li/Air Batteries. **Journal of The Electrochemical Society**, v. 159, n. 2, p. R1–R30, 2011.

EDENHOFER, O. et al. **IPCC, 2014: Climate Change 2014: Mitigation of Climate Change. Contribution of Working Group III to the Fifth Assessment Report of the**

Intergovernmental Panel on Climate Change. [s.l: s.n.].

FAUNCE, T. A. et al. On-grid batteries for large-scale energy storage: Challenges and opportunities for policy and technology. **MRS Energy & Sustainability**, v. 5, n. May 2020, p. 1–12, 2018.

FENG, N.; HE, P.; ZHOU, H. **Critical Challenges in Rechargeable Aprotic Li-O2 BatteriesAdvanced Energy Materials**, 2016. .

FIATES, J. **Understanding The Role Of Electrolytes And Electrodes On Li-Air Batteries Through Molecular Dynamics Simulation**. Tese (Doutorado em Engenharia Química) - Faculdade de Engenharia Química, Universidade de Campinas. Campinas. p. 172. 2020.

FIATES, J. et al. Impact of anion shape on Li+solvation and on transport properties for lithium-air batteries: a molecular dynamics study. **Physical Chemistry Chemical Physics**, v. 22, n. 28, p. 15842–15852, 2020.

FREUNBERGER, S. a. et al. Reactions in the rechargeable lithium-O2 battery with alkyl carbonate electrolytes. **Journal of the American Chemical Society**, v. 133, n. 20, p. 8040–8047, 2011a.

FREUNBERGER, S. A. et al. The Lithium-Oxygen Battery with Ether-Based Electrolytes. **Angewandte Chemie International Edition**, v. 50, n. 37, p. 8609–8613, 2011b. Disponível em: <http://doi.wiley.com/10.1002/anie.201102357>.

GAO, X. et al. A rechargeable lithium–oxygen battery with dual mediators stabilizing the carbon cathode. **Nature Energy**, v. 2, p. 17118, 2017. Disponível em: <http://www.nature.com/articles/nenergy2017118>.

GIRISHKUMAR, G. et al. Lithium-air battery: Promise and challenges. **Journal of Physical Chemistry Letters**, v. 1, n. 14, p. 2193–2203, 2010.

GITTLESON, F. S. et al. Catalyst and electrolyte synergy in Li–O2 batteries. **Physical Chemistry Chemical Physics**, v. 16, n. 7, p. 3230–3237, 2014. Disponível em: <http://xlink.rsc.org/?DOI=c3cp54555e>.

GITTLESON, F. S. et al. Raman Spectroscopy in Lithium-Oxygen Battery Systems. **ChemElectroChem**, v. 2, n. 10, p. 1446–1457, 2015.

GITTLESON, F. S. et al. Oxygen solubility and transport in Li-air battery electrolytes: Establishing criteria and strategies for electrolyte design. **Energy and Environmental Science**, v. 10, n. 5, p. 1167–1179, 2017.

GITTLESON, F. S.; RYU, W. H.; TAYLOR, A. D. Operando observation of the gold-electrolyte interface in Li-O2 batteries. **ACS Applied Materials and Interfaces**, v. 6, n.

21, p. 19017–19025, 2014.

GOTTFRIED, J. M. Surface chemistry of porphyrins and phthalocyanines. **Surface Science Reports**, v. 70, n. 3, p. 259–379, 2015. Disponível em: <http://dx.doi.org/10.1016/j.surfrep.2015.04.001>.

GOWDA, S. R. et al. Implications of CO2 contamination in rechargeable nonaqueous Li-O2 batteries. **Journal of Physical Chemistry Letters**, v. 4, n. 2, p. 276–279, 2013.

GUO, Z. et al. Humidity effect on electrochemical performance of Li-O2 batteries. **Journal of Power Sources**, v. 264, p. 1–7, 2014. Disponível em: <http://dx.doi.org/10.1016/j.jpowsour.2014.04.079>.

HARBACH, F.; FISCHER, F. Raman spectra of lithium hydroxide single crystals. **Journal of Physics and Chemistry of Solids**, v. 36, n. 6, p. 601–603, 1975.

HUTH, F. et al. Nano-FTIR absorption spectroscopy of molecular fingerprints at 20 nm spatial resolution. **Nano Letters**, v. 12, n. 8, p. 3973–3978, 2012.

IMANISHI, N.; LUNTZ, A. C.; BRUCE, P. **The Lithium Air Battery: Fundamentals**. [s.l: s.n.]v. 1

IZUTSU, K. **Electrodeposition from Ionic Liquids Nanostructured Materials in Electrochemistry Electrochemistry**. [s.l: s.n.]

JO, K. et al. Stable aqueous dispersion of reduced graphene nanosheets via non-covalent functionalization with conducting polymers and application in transparent electrodes. **Langmuir**, v. 27, n. 5, p. 2014–2018, 2011.

KEILMANN, F.; HILLENBRAND, R. Near-field microscopy by elastic light scattering from a tip. **Philosophical Transactions of the Royal Society A: Mathematical, Physical and Engineering Sciences**, v. 362, n. 1817, p. 787–805, 2004.

KO, Y. et al. Redox Mediators: A Solution for Advanced Lithium–Oxygen Batteries. **Trends in Chemistry**, v. 1, n. 3, p. 349–360, 2019a. Disponível em: <https://doi.org/10.1016/j.trechm.2019.03.016>.

KO, Y. et al. Redox Mediators : A Solution for Advanced Lithium – Oxygen Batteries. **Trends in Cognitive Sciences**, v. 1, n. 3, p. 349–360, 2019b. Disponível em: <https://doi.org/10.1016/j.trechm.2019.03.016>.

KWABI, D. G. et al. Chemical instability of dimethyl sulfoxide in lithium-air batteries. **Journal of Physical Chemistry Letters**, v. 5, n. 16, p. 2850–2856, 2014.

KWAK, W.-J. et al. Review—A Comparative Evaluation of Redox Mediators for Li-O $_2$ Batteries: A Critical Review. **Journal of The Electrochemical Society**, v. 165, n. 10, p. A2274–A2293, 2018. Disponível em:

<http://jes.ecsdl.org/lookup/doi/10.1149/2.0901810jes>.

KWAK, W. J. et al. Understanding the behavior of Li-oxygen cells containing LiI. **Journal of Materials Chemistry A**, v. 3, n. 16, p. 8855–8864, 2015.

KWAK, W. J. et al. Li-O2 cells with LiBr as an electrolyte and a redox mediator. **Energy and Environmental Science**, v. 9, n. 7, p. 2334–2345, 2016.

LANDA-MEDRANO, I. et al. Redox mediators: A shuttle to efficacy in metal-O2 batteries. **Journal of Materials Chemistry A**, v. 7, n. 15, p. 8746–8764, 2019.

LAOIRE, C. O. et al. Influence of nonaqueous solvents on the electrochemistry of oxygen in the rechargeable lithium-air battery. **Journal of Physical Chemistry C**, v. 114, n. 19, p. 9178–9186, 2010.

LEE, C. K.; PARK, Y. J. CsI as Multifunctional Redox Mediator for Enhanced Li-Air Batteries. **ACS Applied Materials and Interfaces**, v. 8, n. 13, p. 8561–8567, 2016.

LEE, S. H.; KWAK, W. J.; SUN, Y. K. A new perspective of the ruthenium ion: A bifunctional soluble catalyst for high efficiency Li-O 2 batteries. **Journal of Materials Chemistry A**, v. 5, n. 30, p. 15512–15516, 2017.

LI, Z. et al. Understanding the Electrochemical Formation and Decomposition of Li2O2 and LiOH with Operando X-ray Diffraction. **Chemistry of Materials**, v. 29, n. 4, p. 1577–1586, 2017.

LIANG, Z.; LU, Y. C. Critical Role of Redox Mediator in Suppressing Charging Instabilities of Lithium-Oxygen Batteries. **Journal of the American Chemical Society**, v. 138, n. 24, p. 7574–7583, 2016.

LIM, H. D. et al. Superior rechargeability and efficiency of lithium-oxygen batteries: Hierarchical air electrode architecture combined with a soluble catalyst. **Angewandte Chemie - International Edition**, v. 126, p. 4007–4012, 2014.

LIU, J. et al. Highly efficient Ru/MnO2 nano-catalysts for Li-O2 batteriesQuantitative analysis of catalytic Li2O2 decomposition by operando synchrotron X-ray diffraction. **Journal of Power Sources**, v. 352, p. 208–215, 2017a.

LIU, T. et al. Cycling Li-O2 batteries via LiOH formation and decomposition. **Encyclopedia of Soils in the Environment**, v. 350, n. 6260, p. 530–533, 2015.

LIU, Y. et al. Understanding and suppressing side reactions in Li-air batteries. **Materials Chemistry Frontiers**, v. 1, n. 12, p. 2495–2510, 2017b.

LIU, Z. et al. Carbon-Free O 2 Cathode with Three-Dimensional Ultralight Nickel Foam-Supported Ruthenium Electrocatalysts for Li – O 2 Batteries. v. 8568, p. 2714–2719, 2017c.

LOBO, A. O. et al. Caracterização de materiais carbonosos por espectroscopia raman. **Ceramics**, v. 24, n. 2, p. 98–103, 2005. Disponível em: <http://www2.fc.unesp.br/rbav/index.php/rbav/article/view/99>.

LU, J. et al. A lithium-oxygen battery based on lithium superoxide. **Nature**, v. 529, n. 7586, p. 377–382, 2016. Disponível em: <http://dx.doi.org/10.1038/nature16484>.

LU, Y.-C. et al. Electrocatalytic Activity Studies of Select Metal Surfaces and Implications in Li-Air Batteries. **Journal of The Electrochemical Society**, v. 157, n. 9, p. A1016, 2010a. Disponível em: <http://jes.ecsdl.org/cgi/doi/10.1149/1.3462981>.

LU, Y.-C. et al. In Situ Ambient Pressure X-ray Photoelectron Spectroscopy Studies of Lithium-Oxygen Redox Reactions. **Scientific Reports**, v. 2, n. 1, p. 715, 2012. Disponível em: <http://www.nature.com/articles/srep00715>.

LU, Y. C. et al. Platinum-gold nanoparticles: A highly active bifunctional electrocatalyst for rechargeable lithium-air batteries. **Journal of the American Chemical Society**, v. 132, n. 35, p. 12170–12171, 2010b.

LU, Y. C. et al. Lithium-oxygen batteries: Bridging mechanistic understanding and battery performance. **Energy and Environmental Science**, v. 6, n. 3, p. 750–768, 2013.

LUCAS, I. T. et al. IR near-field spectroscopy and imaging of single LixFePO4 microcrystals. **Nano Letters**, v. 15, n. 1, p. 1–7, 2015.

LYU, Z. et al. Recent advances in understanding of the mechanism and control of Li2O2 formation in aprotic Li-O2 batteries. **Chemical Society Reviews**, v. 46, n. 19, p. 6046–6072, 2017.

MA, X. et al. In situ characterization of electrochemical processes in one dimensional nanomaterials for energy storages devices. **Nano Energy**, v. 24, p. 165–188, 2016. Disponível em: <http://dx.doi.org/10.1016/j.nanoen.2016.03.023>.

MA, Z. et al. A review of cathode materials and structures for rechargeable lithium–air batteries. **Energy Environ. Sci.**, v. 8, n. 8, p. 2144–2198, 2015a. Disponível em: <http://xlink.rsc.org/?DOI=C5EE00838G>.

MA, Z. et al. A review of cathode materials and structures for rechargeable lithium-air batteries. **Energy and Environmental Science**, v. 8, n. 8, p. 2144–2198, 2015b.

MASARAPU, C.; WEI, B. Direct growth of aligned multiwalled carbon nanotubes on treated stainless steel substrates. **Langmuir**, v. 23, n. 17, p. 9046–9049, 2007.

MCCLOSKEY, B. D.; ADDISON, D. A Viewpoint on Heterogeneous Electrocatalysis and Redox Mediation in Nonaqueous Li-O2Batteries. **ACS Catalysis**, v. 7, n. 1, p. 772–778, 2017.

MITCHELL, R. R. et al. All-carbon-nanofiber electrodes for high-energy rechargeable Li–O2 batteries. **Energy & Environmental Science**, v. 4, n. 8, p. 2952, 2011. Disponível em: <http://xlink.rsc.org/?DOI=c1ee01496j>.

MIZUNO, F. et al. Rechargeable Li-Air Batteries with Carbonate-Based Liquid Electrolytes. **Electrochemistry**, v. 78, n. 5, p. 403–405, 2010. Disponível em: <http://repositorio.unan.edu.ni/2986/1/5624.pdf>.

MOZHZHUKHINA, N.; MÉNDEZ DE LEO, L. P.; CALVO, E. J. Infrared spectroscopy studies on stability of dimethyl sulfoxide for application in a Li-air battery. **Journal of Physical Chemistry C**, v. 117, n. 36, p. 18375–18380, 2013.

MULLER, E. A. et al. Infrared vibrational nano-crystallography and nano-imaging. **SCIENCE ADVANCES**, v. 2, p. 1–7, 2016.

NAKANISHI, A. et al. Electrolyte Composition in Li/O2 Batteries with LiI Redox Mediators: Solvation Effects on Redox Potentials and Implications for Redox Shuttling. **Journal of Physical Chemistry C**, v. 122, n. 3, 2018.

Nonaqueous Electrochemistry. [s.l: s.n.]

PARK, J. B. et al. Redox Mediators for Li–O2Batteries: Status and Perspectives. **Advanced Materials**, v. 30, n. 1, p. 1–13, 2018.

PARK, M. et al. Lithium-Air Batteries: Survey on the Current Status and Perspectives Towards Automotive Applications from a Battery Industry Standpoint. **Advanced Energy Materials**, v. 2, n. 7, p. 780–800, 2012. Disponível em: <http://doi.wiley.com/10.1002/aenm.201200020>.

PENG, Z. et al. Oxygen reactions in a non-aqueous Li+ electrolyte. **Angewandte Chemie - International Edition**, v. 50, n. 28, p. 6351–6355, 2011.

PRZYWARSKA-BONIECKA, H.; TRYNDA, L.; ANTONINI, E. Complexes of Metal Phthalocyanines with Globin as the Models of Heme Proteins. **European Journal of Biochemistry**, v. 52, n. 3, p. 567–573, 1975.

QIAO, Y. et al. Unraveling the Complex Role of Iodide Additives in Li-O2 Batteries. **ACS Energy Letters**, v. 2, n. 8, p. 1869–1878, 2017.

QIAO, Y.; YE, S. Spectroscopic Investigation for Oxygen Reduction and Evolution Reactions with Tetrathiafulvalene as a Redox Mediator in Li-O2 Battery. **Journal of Physical Chemistry C**, v. 120, n. 29, p. 15830–15845, 2016.

READ, J. Characterization of the Lithium/Oxygen Organic Electrolyte Battery. **Journal of The Electrochemical Society**, v. 149, n. 9, p. A1190–A1195, 2002.

RINALDI, A. et al. Lithium-air batteries for medium- and large-scale energy storage. In:

Advances in Batteries for Medium and Large-Scale Energy Storage: Types and Applications. [s.l.] Elsevier Ltd., 2015. p. 387–440.

RYAN, K. R. et al. In situ synchrotron X-ray diffraction studies of lithium oxygen batteries. p. 6915–6919, 2013.

RYU, W.-H. et al. Heme biomolecule as redox mediator and oxygen shuttle for efficient charging of lithium-oxygen batteries. **Nature Communications**, v. 7, n. 1, 2016.

SCHROEDER, M. A. et al. DMSO-Li2O2 interface in the rechargeable Li-O2 battery cathode: Theoretical and experimental perspectives on stability. **ACS Applied Materials and Interfaces**, v. 7, n. 21, p. 11402–11411, 2015.

SCHWENKE, K. U. et al. The influence of water and protons on Li2O2 crystal growth in aprotic Li-O2 cells. **Journal of the Electrochemical Society**, v. 162, n. 4, p. A573–A584, 2015.

SHAO, Y. et al. Electrocatalysts for nonaqueous lithium-air batteries: Status, challenges, and perspective. **ACS Catalysis**, v. 2, n. 5, p. 844–857, 2012.

SHARON, D. et al. Oxidation of dimethyl sulfoxide solutions by electrochemical reduction of oxygen. **Journal of Physical Chemistry Letters**, v. 4, n. 18, p. 3115–3119, 2013.

SHUI, J. et al. Reversibility of anodic lithium in rechargeable lithium–oxygen batteries. **Nature Communications**, v. 4, p. 1–7, 2013. Disponível em: <http://dx.doi.org/10.1038/ncomms3255>.

SMITH, E.; DENT, G. **Modern Raman spectroscopy—a practical approach**. [s.l: s.n.]v. 36

STORM, M. M. **Preparation and Characterization of Cathode Materials for Lithium-Oxygen Batteries**. 2016. Technical University of Denmark, 2016.

SUN, D. et al. A solution-phase bifunctional catalyst for lithium-oxygen batteries. **Journal of the American Chemical Society**, v. 136, n. 25, p. 8941–8946, 2014.

SUN, J. et al. A rechargeable Li-air fuel cell battery based on garnet solid electrolytes. **Scientific Reports**, v. 7, n. 8, p. 1–8, 2017. Disponível em: <http://dx.doi.org/10.1038/srep41217>.

SZUBZDA, B.; SZMAJA, A.; HALAMA, A. Influence of structure and wettability of supercapacitor electrodes carbon materials on their electrochemical properties in water and organic solutions. In: Electrochimica Acta, **Anais**...Pergamon, 30 dez. 2012. Disponível em: <https://www.sciencedirect.com/science/article/pii/S0013468612013503>. Acesso em:

25 out. 2018.

TO, J. W. F. et al. Ultrahigh surface area three-dimensional porous graphitic carbon from conjugated polymeric molecular framework. **ACS Central Science**, v. 1, n. 2, p. 68–76, 2015.

TUŁODZIECKI, M. et al. The role of iodide in the formation of lithium hydroxide in lithium-oxygen batteries. **Energy and Environmental Science**, v. 10, n. 8, p. 1828–1842, 2017.

VAN KRANENDONK, J. Intermolecular spectroscopy. In: **Physica**. [s.l: s.n.]73p. 156–173.

VIRWANI, K. et al. In situ AFM visualization of Li–O 2 battery discharge products during redox cycling in an atmospherically controlled sample cell. **Beilstein Journal of Nanotechnology**, v. 10, p. 930–940, 2019.

VISWANATHAN, V. et al. Electrical conductivity in Li 2O 2 and its role in determining capacity limitations in non-aqueous Li-O 2 batteries. **Journal of Chemical Physics**, v. 135, n. 21, 2011.

VIVEK, J. P. et al. In Situ Surface-Enhanced Infrared Spectroscopy to Identify Oxygen Reduction Products in Nonaqueous Metal-Oxygen Batteries. **Journal of Physical Chemistry C**, v. 121, n. 36, p. 19657–19667, 2017.

WAGNER, F. T.; LAKSHMANAN, B.; MATHIAS, M. F. Electrochemistry and the Future of the Automobile. **The Journal of Physical Chemistry Letters**, v. 1, n. 14, p. 2204–2219, 2010. Disponível em: <http://pubs.acs.org/doi/abs/10.1021/jz100553m>.

WANG, G. et al. Understanding Moisture and Carbon Dioxide Involved Interfacial Reactions on Electrochemical Performance of Lithium-Air Batteries Catalyzed by Gold/Manganese-Dioxide. **ACS Applied Materials and Interfaces**, v. 7, n. 43, p. 23876–23884, 2015.

WANG, M. The Greenhouse Gases , Regulated Emissions , and Energy Use in Transportation (GREET) Model Version 1 . 5. **Environmental Protection**, p. 1–8, 1999.

WANG, Y. et al. A Solvent-Controlled Oxidation Mechanism of Li2O2 in Lithium-Oxygen Batteries. **Joule**, v. 2, n. 11, p. 2364–2380, 2018. Disponível em: <https://doi.org/10.1016/j.joule.2018.07.021>.

WANG, Y. et al. Critical Factors Controlling Superoxide Reactions in Lithium–Oxygen Batteries. **ACS Energy Letters**, v. 5, n. 5, p. 1355–1363, 2020.

WANG, Z. et al. Vibrational spectroscopic study of the interaction between lithium perchlorate and dimethylsulfoxide. **Electrochimica Acta**, v. 42, n. 17, p. 2611–2617,

1997.

WEN, Z.; SHEN, C.; LU, Y. Air electrode for the lithium-air batteries: Materials and structure designs. **ChemPlusChem**, v. 80, n. 2, p. 270–287, 2015.

XIAO, J. et al. Optimization of Air Electrode for Li/Air Batteries. **Journal of The Electrochemical Society**, v. 157, n. 4, p. A487, 2010.

XIAO, J. et al. Hierarchically porous graphene as a lithium-air battery electrode. **Nano Letters**, v. 11, n. 11, p. 5071–5078, 2011.

XIN, X.; ITO, K.; KUBO, Y. Highly Efficient Br-/NO3- Dual-Anion Electrolyte for Suppressing Charging Instabilities of Li-O2 Batteries. **ACS Applied Materials and Interfaces**, v. 9, n. 31, p. 25976–25984, 2017.

XU, D. et al. Novel DMSO-based electrolyte for high performance rechargeable Li–O2 batteries. **Chemical Communications**, v. 48, p. 6948–6950, 2012.

YOUNESI, R. **Characterization of Reaction Products in the Li-O 2 Battery Using Photoelectron Spectroscopy**. 2012. 2012.

ZHANG, S. S.; FOSTER, D.; READ, J. Discharge characteristic of a non-aqueous electrolyte Li/O 2 battery. **Journal of Power Sources**, v. 195, n. 4, p. 1235–1240, 2010. Disponível em: <http://www.scopus.com/inward/record.url?eid=2-s2.0-71549117652&partnerID=tZOtx3y1>.

ZHANG, T.; ZHOU, H. A reversible long-life lithium-air battery in ambient air. **Nature Communications**, v. 4, n. May, p. 1–7, 2013.

ZHENG, J. P. et al. The Theoretical Energy Densities of Dual-Electrolytes Rechargeable Li-Air and Li-Air Flow Batteries. **Journal of The Electrochemical Society**, v. 158, n. 1, p. A43–A46, 2011. Disponível em: <http://jes.ecsdl.org/cgi/doi/10.1149/1.3515330>.

ZHOU, W. et al. Fundamentals of scanning electron microscopy (SEM). In: **Scanning Microscopy for Nanotechnology: Techniques and Applications**. [s.l: s.n.]p. 1–40.

ZHU, Y. G. et al. Proton enhanced dynamic battery chemistry for aprotic lithium-oxygen batteries. **Nature Communications**, v. 8, p. 4–11, 2017.